

LUMINOUS ASYMPTOTIC GIANT BRANCH STARS IN THE LARGE MAGELLANIC CLOUD¹

NEILL REID, CHRIS TINNEY, AND JEREMY MOULD
 California Institute of Technology

Received 1989 March 29; accepted 1989 July 1

ABSTRACT

We present the results of a search for optically obscured asymptotic giant branch (AGB) stars in the Large Magellanic Cloud (LMC), combining data obtained using the *IRAS* satellite with near-infrared photographic plate material of a 15 deg² region in the northern LMC. Of the 156 *IRAS* sources that are detected either in separate cross-scans or in more than one passband, 63 have [12 – 25] colors consistent with their being either stellar photospheres or circumstellar dust shells. Seventeen of these we identify with bright ($I_c < 9$) foreground stars in our own Galaxy, while a further 17 are associated with red supergiants in the LMC. Of the remaining stars, no more than five are likely to be optically visible AGB stars, while the rest have no obvious optical counterpart. This immediately rules out the presence of sufficient high-luminosity “cocoon” stars to explain the observed deficit of several hundred luminous ($M_{\text{bol}} < -6$) AGB stars between the predictions of standard models of AGB evolution and the observed luminosity function. It remains possible that most of the unidentified sources are dusty AGB stars, evolving through a phase of enhanced mass loss toward becoming planetary nebulae. We infer bolometric magnitudes as low as $M_{\text{bol}} \sim -5$ for these sources and suggest that this phase can be triggered at low luminosities, truncating AGB evolution and leading to the observed scarcity of asymptotic giant branch stars with bolometric magnitudes brighter than -6.0 mag.

Subject headings: galaxies: Magellanic clouds — galaxies: stellar content — infrared: sources — stars: evolution — stars: late-type — stars: long-period variables

I. INTRODUCTION

Asymptotic giant branch (AGB) stars can achieve extremely high luminosities. Descended from intermediate-mass ($0.8 M_{\odot} \leq M_i \leq 6-9 M_{\odot}$) main-sequence stars, these double shell burning giants can dominate the luminosity, particularly in the red and infrared, produced by an intermediate-age (1 to several Gyr) stellar population. On the upper AGB, these stars undergo thermal pulsations and can experience the shorter term atmospheric pulsations that lead to the characteristic light variations of the Mira variables. As both luminous and easily recognizable objects, Mira variables are potentially important as distance indicators to nearby systems. Moreover, AGB stars dredge up carbon and *s*-process elements (such as Ba and Zr), altering the photospheric abundances, and expel these materials into the interstellar medium (ISM) through the mass loss that occurs both during the thermally pulsing stage of evolution and immediately prior to planetary nebula formation. Thus, AGB stars are important in understanding the chemical evolution of the ISM.

Studies of the evolution of AGB stars in the Magellanic Clouds have provided a classic example of the traditional concept of the scientific method. Theoretical predictions are made from the best available models, confronted with observational evidence, and, after debate and empirical verification, the theory is modified, where necessary, to account for the observational data. The initial comparison between the Blanco, McCarthy, and Blanco (1980; hereafter BMB) carbon star surveys and the theoretical models (Iben and Renzini 1983) highlighted two problem areas that have since become familiar as the two aspects of the “carbon star mystery” (Iben 1981). First, many low-luminosity ($M_{\text{bol}} > -4$) carbon stars

were observed that had not been predicted. Second, few of the numerous high-luminosity ($M_{\text{bol}} < -5.5$) carbon stars that are predicted by the models are present among the observed AGB stars.

The luminosity of a star on the AGB is a direct function of the mass of the degenerate core (Paczynski 1970) and the maximum luminosity is set either by the removal of the outer envelope and the formation of a planetary nebula, or by the core mass reaching the Chandrasekhar limit (at $M_{\text{bol}} \sim -7.1$). Thus, the more massive the star, the higher the ascent on the AGB, with all AGB stars more luminous than $M_{\text{bol}} = -6$ being descended from main-sequence stars more massive than $\sim 3 M_{\odot}$. The theoretical predictions are illustrated in Figure 1, taken from Mould and Aaronson (1986), which compares the theoretically predicted variation of $M_{\text{bol}}(\text{max})$ as a function of initial mass with the relation that is inferred from observations of Magellanic Cloud globular clusters. Mass loss is included, using the standard Reimers (1975) approximation.

The existence of carbon stars at low luminosities thus implies that the original theoretical models underestimated the lower mass limit for carbon dredge-up. Indeed, prior to the BMB surveys, Zuckerman *et al.* (1978) had suggested that, since C-rich planetaries were descended from relatively low-mass ($\sim 1.1 M_{\odot}$) stars, the theoretical lower limit of $2 M_{\odot}$ for mixing of nucleosynthesis products must indicate some deficiency in the models. Subsequent analysis has shown that convection does occur more readily in the models, permitting dredge-up and pushing the C/O ratio in the photosphere above unity (Iben and Renzini 1982; Lattanzio 1988).

The absence of luminous carbon stars is more problematic. Iben (1981) originally proposed four methods of hiding these stars from the BMB survey: first, a pause in the star formation rate and a consequent absence of young, massive stars; second, “envelope” or “hot bottom” burning, whereby carbon is converted to nitrogen at the base of the convective layer, reducing

¹ Based on data obtained using the *Infrared Astronomical Satellite* and on observations obtained at the Las Campanas Observatory of the Carnegie Institution of Washington.

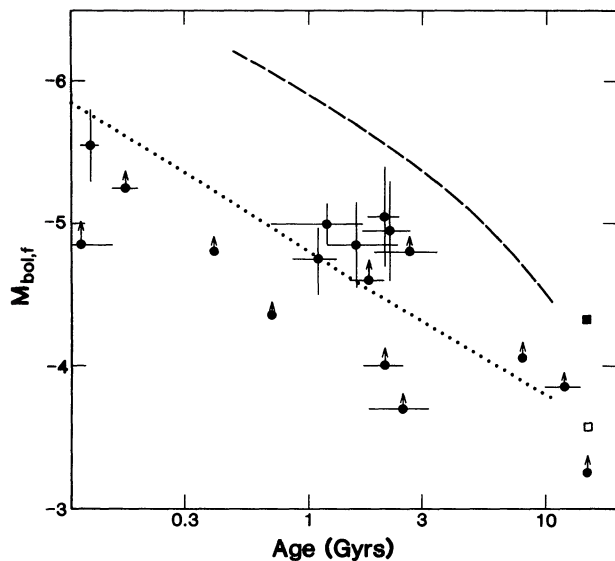


FIG. 1.—Relationship between the maximum luminosity on the asymptotic giant branch and initial mass. Dashed line is the theoretically predicted relation, which is matched against observations in LMC clusters of known age (Mould and Aaronson 1986). Dotted line is the locus of thermal pulse ignition of the AGB according to Iben and Renzini 1983.

C/O to less than 1 and turning a carbon star into an S-type giant; third, additional mass loss on the upper AGB and early planetary nebula formation; fourth, the formation of “cocoon” stars, giants heavily enshrouded in circumstellar dust shells and invisible to optical surveys. Finally, Renzini *et al.* (1985) and Castellani *et al.* (1985*a, b*) offered a fifth partial solution—reducing from $9 M_{\odot}$ to $5\text{--}6 M_{\odot}$ the upper limit for entry onto the AGB.

Taking these proposals in turn, Cepheids are the immediate precursors of the more luminous AGB stars ($M_i > 3 M_{\odot}$). Thus, an irregularity in the star formation history should be reflected by a scarcity of Cepheids. Conversely, given Cepheid and AGB models, one should be able to infer the expected number of luminous AGB stars from the period distribution of the variable stars. Becker (1982) applied this analysis to several of the BMB fields and concluded that all showed evidence for recent star formation—that is, there were Cepheids in each field, thus there should have been bright AGB stars. We shall discuss the Cepheid distribution in the LMC (north) field in § III.

The BMB grism surveys were optimized for the discovery of carbon stars and late-type M giants, and become increasingly incomplete for earlier type M giants. However, the photographic surveys carried out by Reid and Mould (1984; hereafter RM84) and Reid, Mould, and Thompson (1987; hereafter RMT87) select AGB stars using $V-I$ colors and have been used to construct complete samples including both early- and late-type M giants, in addition to the redder carbon stars. As we discuss further in § II, the luminosity function derived from these studies remains deficient in luminous AGB stars. Indeed, Reid and Mould (1985) have suggested that a significant fraction of the luminous M stars that are observed are young, core-helium burning (CHB) supergiants (mass $\sim 10 M_{\odot}$), rather than second giant branch stars.

Of the other proposed explanations, reducing the upper mass limits of the AGB star progenitors is but a partial solu-

tion, because even a $5 M_{\odot}$ star is expected to achieve $M_{\text{bol}} \sim -7$. Both the remaining options invoke mass loss, either to hide the star or to remove it prematurely from the AGB track. In the latter case, either continuous mass loss or the triggering of a “superwind” phase leading to ejection of the envelope and planetary nebula formation at some threshold luminosity is possible. Clearly, the “cocoon” stars can be expected to have strong infrared excesses, and, depending on the extent and duration of the higher mass loss phase, this may also be true in the latter case. Frogel and Richer (1983) surveyed $\sim 67\%$ of the BMB “Bar West” field at $2 \mu\text{m}$, searching for such stars. They failed to find any objects not visible at optical wavelengths, but their scans do not have sufficient sensitivity to exclude the presence of stars similar to the cooler Galactic OH/IR stars. Such objects would, however, be easily detected in the *IRAS* survey data covering the LMC.

In this paper, we report the results of our search for highly obscured, luminous AGB stars lying within a 15 deg^2 region or the northern LMC. We have combined the photographic V - and I -band data discussed in RM84 with analysis of the *IRAS* scans covering the same field. Choosing the subset of *IRAS* sources that have colors corresponding to those of Galactic giants with circumstellar dust emission, we have searched for likely optical counterparts and, where possible, obtained follow-up spectroscopy. In the following sections, we review first the optical derivations of the AGB luminosity function in this field, and go on to consider the period distribution of the Cepheid stars and the implied mass distribution and star formation history. Before discussing the analysis of the *IRAS* data of § V, we consider the properties that LMC cocoon stars might have. Section VI outlines our selection of candidate luminous AGB stars from the catalog of *IRAS* sources, and § VII describes spectroscopic observations of some of these stars. In § VIII, we discuss separately a group of LMC red supergiants which were detected by *IRAS*, *IRAS* sources with no obvious optical counterpart, and the surviving AGB candidates. Section IX summarizes our conclusions.

II. OPTICALLY IDENTIFIED LUMINOUS AGB STARS IN THE LMC (NORTH) FIELD

The region of the LMC covered in the RM84 photographic survey extends from $\sim 5 \text{ hr}$ right ascension to $\sim 5^{\text{h}}45^{\text{m}}$, with the southern limit at $\sim -68^{\circ}20'$; that is, running from approximately 1° north of 30 Dor to just above the western end of the Bar. The boundaries were chosen to minimize crowding problems. However, the star-forming region Shapley III lies within the field, and, to simplify the analysis, this area was analyzed separately using photographic plates taken on the du Pont 2.5 m (RMT87) Table 1 presents the AGB star luminosity functions derived from these two studies, where we include all stars with $V-I > 1.6$ and calculate the bolometric magnitudes using Bessel and Wood’s (1984) formula

$$BC_I = 0.3 + 0.38(V-I) - 0.14(V-I)^2.$$

The color-magnitude diagrams for the two data sets are presented in Figure 2. The concentration of luminous red giants near Shapley III is obvious, and Mould and Reid (1987) have suggested that many are likely to be young supergiants associated with the recent ($\sim 20 \times 10^6 \text{ yr}$) starburst. Disregarding this possibility for the moment, these starcounts set an upper limit to the extent of the luminous AGB star population.

Mould and Reid (1987) have used *JHK* photometry of a number of AGB stars to check the bolometric calibration and

TABLE 1
THE AGB LUMINOSITY FUNCTION
FROM OPTICAL DATA^a

M_{bol}	Shapley III	LMC (N)	Total
-6.875.....	12	18	30
-6.625.....	10	11	21
-6.375.....	11	11	22
-6.125.....	20	20	40
-5.875.....	18	27	45
-5.625.....	10	38	48
-5.375.....	6	64	70
-5.125.....	3	93	96
-4.875.....	14	158	172
-4.625.....	19	327	346

^a The luminosity function of LMC asymptotic giant branch stars, derived from the V - and I -band photographic surveys by Reid and Mould in the LMC (north) field (excluding Shapley III) and by Reid, Mould, and Thompson in the Shapley III star formation area. The combined luminosity function represents an upper limit to the number of luminous AGB stars, because many of the red giants are late-K/early-M stars, more likely to be young, massive supergiants.

have found that for nonvariable M- and S-type AGB stars the relation is good to $\sim 5\%$. These observations are presented and discussed in the Appendix to this paper. However, a significant fraction of the stars on the asymptotic giant branch are variable. There are larger uncertainties in the total flux in the case of these latter stars, as can be seen by comparing the bolometric magnitudes given for Harvard variables in Table 5 of RM85 with those quoted by Wood, Bessell, and Fox (1981; hereafter WBF). (Note that HV 2555 is misidentified in RM85; the magnitudes quoted are those of an AGB star 1' north of HV 2555).

The RM84 survey was based on five I band plates, taken over a 3 yr period, while WBF obtained JHK photometry of the stars, at several epochs in most cases, and their results are clearly preferred. These discrepancies, the largest of which (allowing for the different distance moduli adopted in the two papers) is 0.9 mag (HV 1001), stem from uncertainties in the I

band magnitudes in the photographic survey. Reid, Glass, and Catchpole (1987; hereafter RGC), however, have used 23 I -band UK Schmidt plates to search for Mira variables in the same field, with infrared JHK photometry being obtained for individual stars. Comparing the bolometric magnitudes derived by the latter authors with the WBF values, the dispersion is ± 0.19 mag. Only 10 of ~ 120 of the long-period variables in this survey have bolometric magnitudes that exceed -6.0 , seven of which were included in the original RM84 sample. Nonetheless, as Hughes and Wood (1988) emphasize, these stars confirm that *some* AGB stars reach luminosities close to the theoretical limit. We note that while a minority of these stars show S-star characteristics, none are carbon stars. In any event, within the full LMC (north) field, optical observations find no more than 116 AGB candidates with luminosities in the range $-6 \leq M_{\text{bol}} \leq -7$. Clearly, these observations cannot take account of the possible presence of longer wavelength radiation from circumstellar dust. We return to this point in § VIII.

III. CEPHEID STARS IN THE LMC (NORTH)

Payne-Gaposkin (1971; hereafter PG71) has cataloged 1111 Cepheid variables in the LMC, giving period determinations in addition to positions. This catalog was used by Becker (1982) in his study of the BMB fields, and our investigation follows the techniques used in that paper.

In PG71, the positions of the Cepheids are given in terms of the Harvard (x, y) system, based on Leavitt's (1906) original photographic plates, but Wesselink (1959) has derived formulae to convert between this system and equatorial coordinates for equinox 1875.0. Using the latter relations, we find that the right ascension limits correspond to x values of 2000–3500 (5^{h}) and from 18,000 to 19,500 in the east, while the declination limits are $y \sim 13,000$ (south) to $\sim 27,000$ (north). For simplicity, we have adopted limits of $2500 \leq x \leq 19,000$ together with the cited y limits in defining the Cepheid sample.

Figure 3 shows the period distribution of PG71 Cepheids that fall within our field and compares this distribution with that shown by the complete sample. The two are clearly similar—the LMC (north) sample is not biased toward the

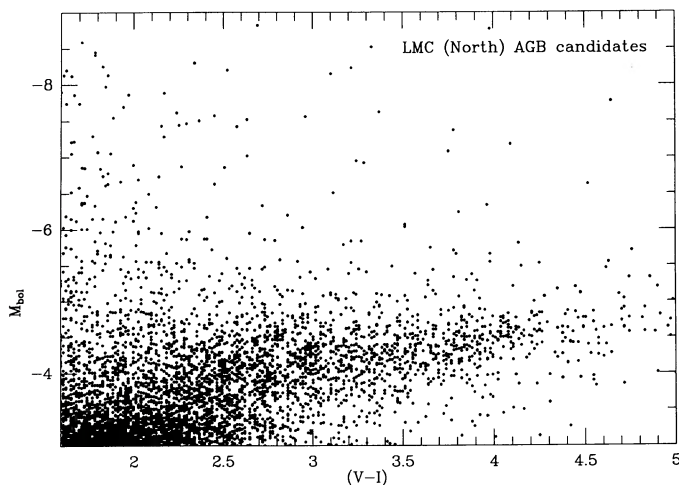


FIG. 2a

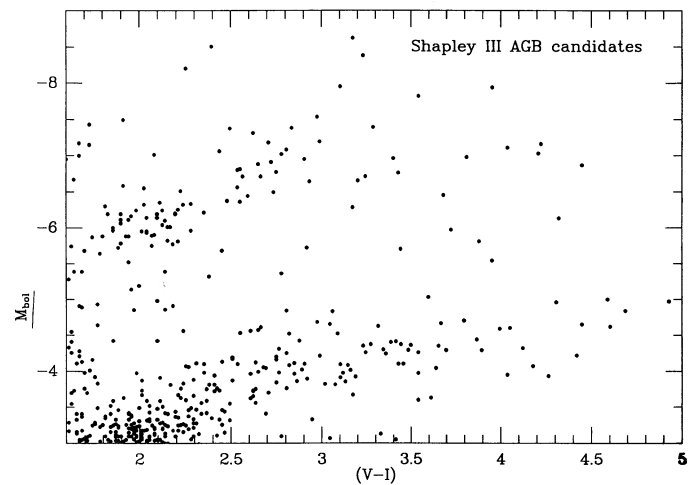


FIG. 2b

FIG. 2.—($M_{\text{bol}}, V - I$) color-magnitude diagrams (a) for the LMC (north) field, excluding the region in the immediate vicinity of Shapley III, and (b) for the area of Shapley Constellation III surveyed using the Las Campanas du Pont telescope. A distance modulus of 18.4 is assumed, and all bolometric corrections are calculated using the formula given in § II, which is appropriate for K and M stars.

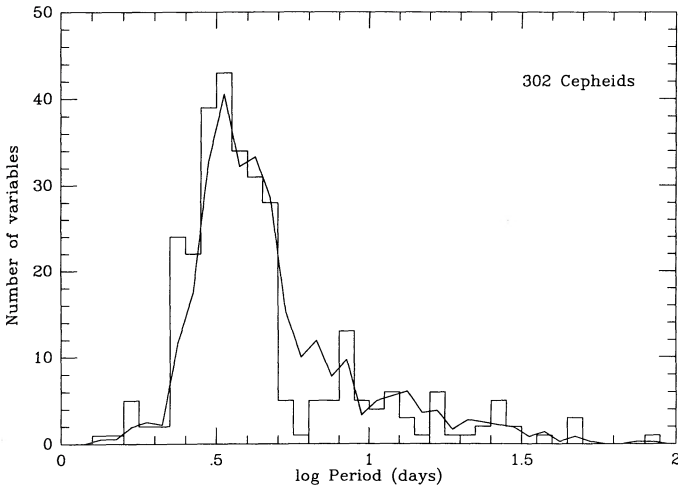


FIG. 3.—Histogram shows the period distribution of the Cepheids cataloged by Payne-Gaposchkin within the LMC (north) field. We also plot as a solid line the distribution of the complete sample of PG Cepheids, scaling the data to the proportions of the LMC (north) sample.

shorter period, lower mass stars. We note in passing that the PG71 sample is known to be incomplete and biased toward long period ($P > 10^d$) stars (Becker, Iben, and Tuggle, 1977; hereafter BIT), and that this may enhance the longer period tail by perhaps a factor of 2. As will become apparent, this is not important for our analysis. However, it appears that *increased* recent star formation is necessary if one is to account for all the long-period stars (BIT).

Following Becker (1982), we can estimate the Cepheid masses by adopting values for the heavy metal and helium abundances in the LMC (in this case, $Y = 0.25$ and $Z = 0.01$), and applying equations (13), (16), (17), and (18) from BIT. This assumes that the variables are being observed on their second (or later) crossing of the instability strip, after evolution up the first red giant branch. At this metallicity, stars less massive than $\sim 4 M_{\odot}$ fail to intersect the instability strip during the post-helium flash blue excursions, and this appears to be reflected in Figure 3, where the short-period edge of the broad peak occurs at $\log P \sim 0.35$ or a mass of $\sim 4.3 M_{\odot}$. Most of the

stars (222) lie within the range $0.35 < \log P < 0.7$, corresponding to $\sim 4 M_{\odot} < M < \sim 6$. (BIT comment that, for the most part, the dispersion in the period-mass relation is only $\sim 0.6 M_{\odot}$.) The upper mass limit for AGB progenitors (that is, the lower mass limit for nondegenerate carbon ignition) is still a matter of some debate, but probably lies in the range $7-8 M_{\odot}$ ($0.97-1.1$ in $\log P$). Thus, a further 30-40 Cepheids, making a total of ~ 250 stars, can be expected to become AGB stars in later life.

In order to estimate the number of luminous AGB stars corresponding to the observed Cepheid mass distribution, it is necessary to know the relative lifetimes of the two evolutionary phases. Theory (Renzini 1977) has established the rate of AGB evolution as

$$\Delta t \sim 1.3 \times 10^6 \Delta M_{\text{bol}} \text{ yr}.$$

From Figure 1, it is clear that conventional assumptions about mass loss predict that all stars more massive than $\sim 5 M_{\odot}$ should remain on the AGB until the core mass reaches Chandrasekhar limit, while $\sim 4.3-5 M_{\odot}$ stars peak at luminosities between $M_{\text{bol}} = -6.5$ and -7 . Thus, an AGB star with a mass $\geq 4.3 M_{\odot}$ is expected to spend at least 10^6 yr with a bolometric luminosity above $M_{\text{bol}} = -6.0$.

In comparison, the time spent by a $5 M_{\odot}$ star in evolving from the tip of the first red giant branch to the AGB is $\sim 1.1 \times 10^7$ yr (BIT). Becker (1982) takes this as an estimate of the Cepheid lifetime. However, only $\sim 5 \times 10^5$ yr are actually spent on the instability strip (assuming that opacity mix II is appropriate to the LMC), while the more massive stars may spend as little as 10^5 yr pulsating. Thus one might expect $\sim 500-600$ luminous AGB stars corresponding to the immediate predecessors of the variables shown in Figure 3. As we discussed in § II, there are at most ~ 115 such stars observed.

Finally, we noted the strong concentration of luminous AGB candidates in the vicinity of Shapley III. Figure 4 shows the spatial distribution of the Cepheid variables, separating the stars into those with periods in the range $0.35 \leq \log P < 0.7$ and those with $0.7 \leq \log P < 1.05$. The former have ages of $7-12 \times 10^7$ yr, while the latter span the interval of $\tau \sim 3-7 \times 10^7$ yr. Neither group is particularly concentrated near regions of recent star formation, which is not surprising,

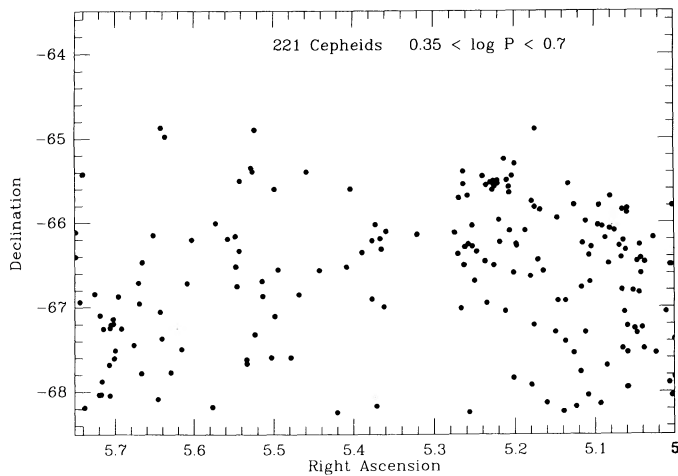


FIG. 4a

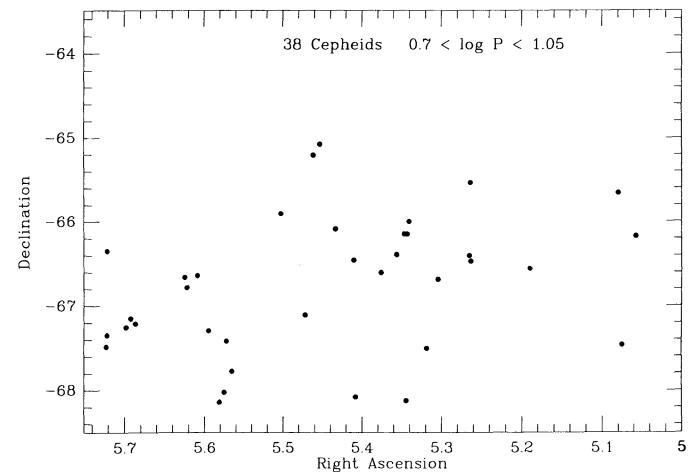


FIG. 4b

FIG. 4.—(a) Spatial distribution of the PG Cepheids. Note the absence of any strong concentration toward Shapley Constellation III. Longer period cepheids are plotted in (b).

because a peculiar motion of only 5 km s^{-1} would suffice to move the youngest variables $10'$ from their birthplace. This again argues in favor of a significant fraction of the Shapley III AGB candidates being supergiants, and suggests that, in reality, the average lifetime of an optically visible luminous ($M_{\text{bol}} < -6$) AGB star is no more than $2 \times 10^5 \text{ yr}$.

IV. THE FAR-INFRARED PROPERTIES OF COCOON STARS

Before describing our analysis of the *IRAS* data, we should consider the expected characteristics of any highly obscured cocoon stars that we might find in the LMC. The *IRAS* satellite obtained data for many Galactic AGB and supergiant stars with substantial circumstellar dust shells. We can use these stars to set the criteria for identifying candidate AGB stars in our survey of the LMC.

Herman, Burger, and Penninx (1986) and Rowan-Robinson *et al.* (1986) have discussed *IRAS* observations of Galactic red giants spanning a wide range of dust-shell properties. In most cases, the circumstellar shell is not optically thick, and the visual to near-infrared colors are little affected. Approximately 10% of the total flux is reradiated at wavelengths beyond $\sim 3 \mu\text{m}$, with the peak of the subsidiary energy distribution lying shortward of $10 \mu\text{m}$. Thus, *IRAS* data for these stars decrease monotonically, in S_{ν} , from 12 to $100 \mu\text{m}$.

A smaller number of stars, however, have substantially denser circumstellar shells, and the flux density distribution peaks at longer wavelengths. Thus, several of the OH/IR stars discussed by Herman, Burger, and Penninx have $S_{\nu}(60) \geq S_{\nu}(25)$, implying equivalent blackbody temperatures as low as $\sim 130 \text{ K}$. The two most extreme sources are *IRAS* 18257–1052 (OH 20.7+0.1) and *IRAS* 18355–0712 (OH 25.1–0.3), with $S_{\nu}(25)/S_{\nu}(60) \sim 0.5$. None of the OH/IR stars have $100 \mu\text{m}$ flux densities that exceed the $60 \mu\text{m}$ values.

Herman, Burger, and Penninx have determined distances to stars in their sample either through direct measurement of the phase lag of variations in the OH line profile and the angular size of the dust shell at radio wavelengths (Herman and Habing 1985), or through applying the ($L_{\text{OH}} - R^2$) relation. Thus, we can use stars from their sample as templates for LMC cocoon stars. In Table 2, we give the expected flux densities for three of the more extreme OH/IR stars, scaling each to an object with a bolometric magnitude of -6.4 at a distance of 48 kpc. $M_{\text{bol}}(*)$ is the actual bolometric magnitude measured by Herman, Burger, and Penninx for each star. Each of these hypothetical high-luminosity AGB stars should be detected comfortably in at least two *IRAS* passbands in the present survey.

Finally, we have made the same calculation for the less extreme stars, taking the well-known carbon star IRC +10216

as the template. Le Bertre (1987) has presented multi-wavelength observations of this object at several phases of the light curve. We can use these data, together with the distance estimate of 130 pc, to estimate that the star has a bolometric magnitude at maximum of $M_{\text{bol}} \sim -5.6$. Thus, in the LMC the star would have a $12 \mu\text{m}$ flux density of $S_{\nu}(12) \sim 0.35 \text{ Jy}$, with the $25 \mu\text{m}$ flux being $\sim 0.17 \text{ Jy}$. The latter datum is close to our detection limit in regions of the LMC unaffected by confusion. With an $I - [12]$ color of 21 mag, the star would be $\sim 12 \text{ mag}$ fainter than the limiting magnitude of our photographic data. Table 2 gives the flux densities appropriate to an $M_{\text{bol}} = -6.4$ star on the upper AGB. Again, such objects should be detected with ease by *IRAS* in the current survey.

V. THE *IRAS* SCANS: DATA ANALYSIS

The infrared observations presented here were obtained as part of the Deep Sky Mapping (DPM) program of *IRAS*. Because the LMC is close to the south ecliptic pole, it was possible for *IRAS* to obtain two separate sets of DPM observations, with almost orthogonal scanning directions running roughly north-south (NS) and east-west (EW). Because of the rectangular shape of the *IRAS* detectors, which achieve maximum resolution in the in-scan direction, the combination of these two data sets provides an effectively circular beam on the LMC of $\sim 0.5'$ at $\lambda = 12$ and $25 \mu\text{m}$ (Beichman *et al.* 1988; hereafter the "Supplement").

The DPM observations of the LMC north field were "coadded" using the DS-GAD software by the *IRAS* Infrared Processing and Analysis Center (IPAC), to produce two sets of LMC grids—one at 12, 25, 60, and $100 \mu\text{m}$ being the sum of all the NS DPM observations, the other being the corresponding EW sum.

The DSGAD software is particularly useful in the context of this study, because it applies spatial point filtering to the DPM grids, in order to suppress the background and enhance the ability to detect and to measure point sources. Since AGB stars in the LMC will be unresolved to *IRAS*, only point sources are of interest in this study. The IPAC software also extracts source data from each resulting "co-add" grid, by selecting all objects having a peak flux greater than 3 times both the median noise for the entire grid and the local noise at the position of the prospective source. (Both the median and local noise estimates are obtained from the local noise grid, which is produced at the same time as each signal grid and which is based on known detector noise characteristics, number of summed observations, etc.) For the final co-added grids from which sources were selected in this survey, the median noise threshold corresponded to a limiting flux density of $\approx 0.08 \text{ Jy}$ at $12 \mu\text{m}$, $\approx 0.07 \text{ Jy}$ at $25 \mu\text{m}$, $\approx 0.2 \text{ Jy}$ at $60 \mu\text{m}$, and $\approx 1.1 \text{ Jy}$ at $100 \mu\text{m}$. However, source extraction is poor in regions of high source density, and the flux limit is only reached in sparsely populated regions. A flux-weighted centroid position and peak flux were determined for each extracted source. Finally, these fluxes were calibrated to the 1984 October standard, as used for the *IRAS Point Source Catalog* (PSC) (1985). Detailed descriptions of the algorithms used by the IPAC "co-adding" software can be found in the Supplement and the Users Guide to the *IRAS* Pointed Observation Products (Young *et al.* 1985; hereafter the "AO Guide").

Because this investigation is interested primarily in studying the stellar components of the LMC, only the 12 and $25 \mu\text{m}$ grids were used in selecting sources as possible AGB objects.

TABLE 2

PREDICTED FAR-INFRARED FLUX DENSITIES
OF LMC COCOON STARS^a

Template	S_{12}	S_{25}	S_{60}	$M_{\text{bol}}(*)$
OH 26.5+0.6	0.50	0.93	0.63	-5.1
OH 32.0-0.5	0.25	0.40	0.68	-7.4
OH 20.7+0.1	0.09	0.28	0.47	-7.9
IRC +10216	0.73	0.35	0.09	-5.6

^a Predicted *IRAS* flux densities for an AGB star of bolometric magnitude -6.4 and an energy distribution similar to the given template star. The actual bolometric magnitude of each of the Galactic stars is given in the final column of this table.

Such a course was dictated both by the desire to search for objects with characteristically warm infrared emission ($T \gtrsim 500$ K), and because the 60 and 100 μm grids suffered severely from source confusion in the LMC and the effects of Galactic foreground emission as a result of infrared "cirrus."

The source lists for objects in both scan directions (EW and NS) and at both 12 and 25 μm were then examined in order to determine the correspondences between single sources detected in each of these four maps. Each source position in each map, in turn, was examined by eye and a list of association drawn up. The decision to do this association by hand rather than automatically was made possible by the small number of infrared sources in the LMC north field ($\lesssim 200$), and allowed us to obtain fluxes for sources confused in only one of the scan directions. Wherever it was possible to obtain also an unconfused 60 or 100 μm association with a source selected at 12 or 25 μm , this was done. Positions and fluxes for all the sources constructed in this way are given in Table 3.

In general, the uncertainties in the flux measurements produced by the *IRAS* additional observations are of order $\pm 15\%$ (AO Guide). However, the uncertainties are very non-Gaussian in this distribution, being largely influenced in crowded regions by the effects of nearby sources. Therefore, although we adopt a general uncertainty of $\pm 15\%$, it should be noted that some sources will be much more uncertain than this. This is especially true for weak sources [$S_{\nu}(12), S_{\nu}(25) \lesssim 0.3$ Jy] and at 60 and 100 μm , where source confusion is a major problem. The source positions quoted in Table 3 should be regarded as good estimates of the source centroid of 30" in the in-scan direction and 90" across-scan. The column labeled "Scan" in Table 3 shows whether a source has been unambiguously detected in only an EW or NS scan, or in both directions. Again, the uncertainties in the position estimates are very non-Gaussian,

which is why we have chosen to use a considerably larger error box than the AO Guide would suggest.

The resultant flux densities, expressed in janskys, have been calculated assuming that the shape of the continuum emission is such that it has constant flux per logarithmic frequency interval; that is,

$$S \propto \nu^{-1}.$$

To convert this flux density into the value appropriate for a given thermal source, it is necessary to apply a temperature-dependent color correction to each *IRAS* band, as detailed in the Supplement. Over the range of temperatures of interest, 2000 K $\gtrsim T \gtrsim 100$ K, this will result in the flux being overestimated by between 0% and 25%. Considering the typical uncertainties in the data described above, and that in general the source temperature is unknown, we have not applied corrections to the data given in Table 3. We have, however, used the appropriate color corrections in our analysis of the objects discussed in § VIII.

We have compared the flux densities derived in our survey of the LMC north field with those derived from Schwering's (1989) analysis of the DPM data base and for those sources contained in the *IRAS* PSC. The ratios of the fluxes as 12 μm for sources common to the TRM and Schwering surveys are shown in Figure 5a, and for sources in the TRM and PSC surveys in Figure 5b. (The corresponding diagrams at 25 μm are similar in form.) The Schwering survey appears to underestimate systematically ($\sim 20\%$ – 30%) the flux density relative to our own measurements, especially at low flux levels. A smaller systematic deviation ($\sim 10\%$) can be seen between our survey and the PSC. The scatter in the TRM/PSC flux ratios is consistent with the photometric uncertainties assumed above.

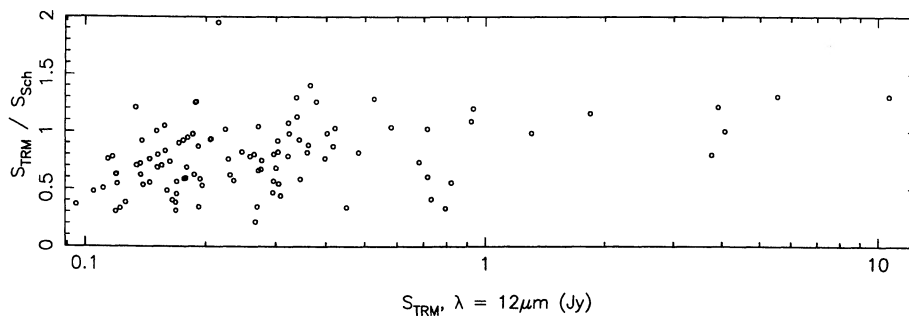


FIG. 5a

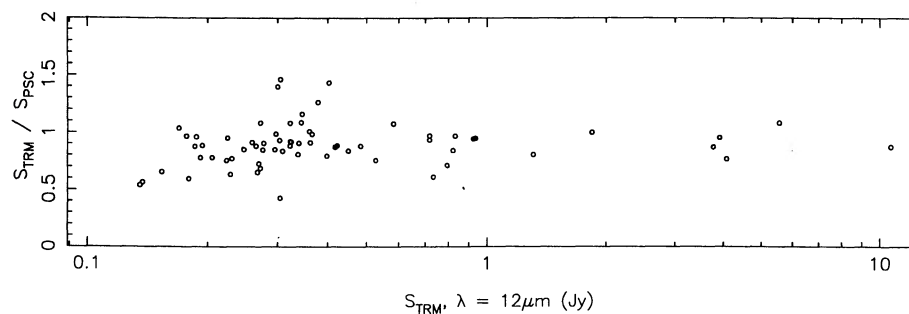


FIG. 5b

FIG. 5.—(a) Ratio of observed flux densities for sources common to the TRM and Schwering (1988) surveys, as a function of TRM flux density. (b) Ratio of observed flux densities for sources common to the TRM and *IRAS* PSC surveys, as a function of TRM flux density.

TABLE 3
TRM SELECTED SOURCES IN LMC NORTH

Source	α	δ	Scan	$S_{12}(Jy)$	$S_{25}(Jy)$	$S_{60}(Jy)$	$S_{100}(Jy)$	PSC	Rej	Comments on Rejection
TRM001	5 23 45.6	-67 55 24	3	0.153	1.158	4.88	-	*	Y	S ₆₀
TRM002	5 22 38.0	-67 56 58	1	0.555	2.080	31.26	-	*	Y	S ₆₀
TRM003	5 20 53.0	-67 55 50	1	0.095	0.266	2.81	-	*	Y	S ₆₀
TRM004	5 11 17.5	-67 55 50	3	0.421	0.289	-	-		N	
TRM005	5 32 47.4	-67 57 3	3	0.527	0.436	-	-	*	N	
TRM006	5 19 41.0	-67 56 2	1	0.189	-	-	-	*	N	
TRM007	5 5 9.9	-67 51 37	1	0.150	-	-	-		N	
TRM008	5 19 24.1	-67 55 0	1	0.378	-	-	-	*	N	
TRM009	5 7 22.0	-67 52 52	3	0.155	0.302	-	-		N	
TRM010	5 43 23.4	-67 50 49	3	0.228	1.064	9.94	315.7	*	Y	S ₁₀₀
TRM011	5 21 37.8	-67 53 53	3	3.905	12.390	31.68	-	*	Y	S ₆₀
TRM012	5 9 26.6	-67 50 56	3	0.135	0.423	-	-		Y	PN
TRM013	5 26 45.6	-67 50 37	1	0.128	0.090	-	-	*	N	
TRM014	5 21 28.8	-67 49 56	1	0.235	1.877	-	-	*	Y	S ₂₅ \gg S ₁₂
TRM015	5 38 29.8	-67 46 58	1	0.119	-	1.42	-	*	Y	S ₆₀
TRM016	5 24 16.4	-67 48 20	3	0.180	0.265	-	-		N	
TRM017	5 22 9.6	-67 49 38	1	0.295	1.734	18.11	-	*	Y	S ₆₀
TRM018	5 35 32.9	-67 45 49	3	0.215	0.303	3.53	-	*	Y	S ₆₀ ,C
TRM019	5 43 56.3	-67 43 27	3	10.660	4.551	-	-	*	N	
TRM020	5 19 3.9	-67 48 4	3	0.338	0.226	-	-		N	
TRM021	5 33 1.4	-67 43 34	1	0.716	3.230	-	-	*	Y	S ₂₅ \gg S ₁₂
TRM022	5 32 36.4	-67 44 11	1	0.732	4.230	50.90	-	*	Y	S ₆₀
TRM023	5 9 58.0	-67 40 14	3	0.176	0.411	0.38	-		N	
TRM024	5 11 18.7	-67 40 6	3	0.265	0.171	-	-		N	
TRM025	5 26 18.0	-67 39 38	3	0.205	0.535	6.54	8.8	*	Y	S ₁₀₀ ,S ₆₀
TRM026	5 22 16.2	-67 37 36	3	0.177	0.534	5.72	-	*	Y	S ₆₀
TRM027	5 35 32.2	-67 36 56	3	3.765	22.900	174.50	287.5	*	Y	S ₁₀₀ ,S ₆₀
TRM028	5 18 37.4	-67 35 27	3	0.206	-	-	-	*	N	
TRM029	5 36 11.9	-67 34 54	1	0.300	1.370	11.70	-	*	Y	S ₆₀
TRM030	5 32 27.7	-67 34 35	3	0.179	0.182	-	-	*	Y	C
TRM031	5 35 8.0	-67 32 22	1	0.211	0.242	-	-	*	Y	C
TRM032	5 13 25.1	-67 32 21	3	0.165	0.215	1.26	-	*	Y	S ₆₀
TRM034	5 25 26.4	-67 32 36	1	0.230	0.604	-	17.3	*	Y	S ₁₀₀
TRM035	5 43 53.2	-67 28 40	3	0.343	0.509	8.22	25.3	*	Y	S ₁₀₀ ,S ₆₀
TRM036	5 14 52.1	-67 30 38	3	0.337	0.227	-	-	*	N	
TRM037	5 26 6.9	-67 31 4	1	0.106	-	-	-		N	
TRM038	5 24 19.6	-67 29 8	3	0.145	0.180	5.57	15.9	*	Y	S ₁₀₀ ,S ₆₀
TRM039	5 33 47.5	-67 26 39	1	0.137	0.086	-	-	*	Y	S ₁₀₀ (u),S ₆₀ (u)
TRM040	5 26 48.0	-67 26 9	1	0.158	-	-	-		N	
TRM041	5 23 37.9	-67 26 55	3	0.193	0.488	7.79	15.7	*	Y	S ₁₀₀ ,S ₆₀
TRM042	5 31 54.1	-67 24 2	1	0.120	0.164	3.12	4.8	*	Y	S ₁₀₀ ,S ₆₀
TRM043	5 12 48.0	-67 23 39	1	0.365	0.310	0.26	-	*	N	
TRM044	5 26 22.4	-67 23 27	3	0.151	0.167	-	-	*	Y	S ₆₀ (u)
TRM045	5 28 21.3	-67 23 13	1	0.134	-	-	-		N	
TRM046	5 30 27.1	-67 21 35	1	0.417	0.239	-	-	*	N	
TRM047	5 16 56.0	-67 22 56	3	0.360	0.611	1.10	26.1	*	Y	S ₁₀₀ ,S ₆₀ ,NGC1895
TRM048	5 4 15.4	-67 20 16	3	0.581	0.274	-	-	*	N	
TRM049	5 29 59.3	-67 20 38	3	0.185	0.123	-	-	*	N	
TRM050	5 30 43.1	-67 19 16	3	0.208	0.123	-	-	*	Y	GC
TRM051	5 3 33.6	-67 15 12	1	0.111	-	-	-		N	
TRM052	5 27 33.5	-67 17 28	1	0.153	-	-	-	*	N	
TRM053	5 14 48.8	-67 14 57	1	0.137	0.364	5.57	12.0	*	Y	S ₁₀₀ ,S ₆₀
TRM054	5 29 22.1	-67 15 40	3	0.275	0.225	-	-	*	Y	PN
TRM055	5 42 46.6	-67 9 37	3	0.157	-	-	-	*	N	
TRM056	5 12 32.4	-67 12 28	3	0.126	0.204	3.20	-	*	Y	S ₆₀
TRM057	5 10 44.3	-67 8 21	3	0.179	0.469	5.91	25.9	*	Y	S ₁₀₀ ,S ₆₀

TABLE 3—Continued

Source	α			δ			Scan	$S_{12}(Jy)$	$S_{25}(Jy)$	$S_{60}(Jy)$	$S_{100}(Jy)$	PSC	Rej	Comments on Rejection
TRM058	5	32	40.5	-67	8	38	1	0.296	0.308	-	-		N	
TRM059	5	23	6.1	-67	9	6	1	0.122	0.107	-	-	*	Y	$S_{60}(u)$
TRM060	5	32	56.0	-67	8	23	1	0.923	1.595	-	-		N	
TRM061	5	36	48.3	-67	5	53	3	0.137	0.131	3.32	-	*	Y	S_{60}
TRM062	5	35	24.5	-67	4	31	3	0.120	0.129	-	-	*	N	
TRM063	5	33	30.3	-67	6	10	3	0.296	0.177	0.30	-	*	N	
TRM064	5	5	19.3	-66	59	2	3	0.482	5.850	29.20	47.8	*	Y	S_{100}, S_{60}
TRM065	5	28	15.4	-67	0	59	3	0.152	-	-	-	*	N	
TRM066	5	30	9.7	-67	0	9	3	0.150	0.214	4.68	12.3	*	Y	S_{100}, S_{60}
TRM067	5	36	28.2	-66	57	28	3	0.324	0.266	-	-	*	N	
TRM068	5	35	32.3	-66	57	55	3	0.303	0.218	-	-	*	N	
TRM069	5	29	37.6	-66	57	35	3	0.186	0.153	-	-	*	N	
TRM070	5	4	44.0	-66	53	9	1	0.119	0.211	3.55	13.8	*	Y	S_{100}, S_{60}
TRM071	5	20	16.4	-66	55	54	3	0.277	1.990	24.15	42.2	*	Y	S_{100}, S_{60}
TRM072	5	11	40.5	-66	54	42	3	0.145	-	-	-		N	
TRM073	5	27	36.5	-66	56	4	3	0.176	0.155	-	-	*	N	
TRM074	5	3	37.8	-66	49	25	3	0.105	0.479	1.33	-	*	Y	$S_{100}(c), S_{60}$
TRM075	5	30	22.8	-66	54	56	3	0.192	0.120	-	-	*	Y	GC NGC2002
TRM076	5	36	59.6	-66	51	26	1	0.138	0.167	2.96	16.4	*	Y	S_{100}, S_{60}
TRM077	5	36	4.6	-66	48	31	3	0.224	0.151	-	-		N	
TRM078	5	33	10.5	-66	50	21	3	0.271	0.192	-	-	*	N	
TRM079	5	30	5.4	-66	51	33	3	0.223	0.146	-	-		N	
TRM080	5	20	34.4	-66	49	31	3	0.271	0.926	15.50	33.1	*	Y	S_{100}, S_{60}
TRM081	5	17	30.4	-66	46	32	3	0.450	4.295	27.90	47.7	*	Y	S_{100}, S_{60}
TRM082	5	23	29.8	-66	45	42	3	0.196	0.138	2.28	-	*	Y	S_{60}
TRM083	5	17	41.0	-66	44	58	3	0.208	0.199	-	-	*	Y	NSO
TRM084	5	38	0.5	-66	41	38	3	0.114	0.222	1.99	12.2	*	Y	S_{100}, S_{60}
TRM085	5	29	7.6	-66	43	32	3	0.322	0.097	-	-	*	N	
TRM086	5	22	49.8	-66	43	42	3	0.308	1.520	11.70	-	*	Y	S_{60}
TRM087	5	31	55.6	-66	42	28	3	0.164	0.117	-	-	*	N	
TRM088	5	20	19.5	-66	38	53	3	0.163	-	-	-		N	
TRM089	5	31	36.4	-66	32	10	3	0.259	0.212	-	-	*	N	
TRM090	5	19	44.0	-66	29	48	3	0.139	-	-	-	*	N	
TRM091	5	10	2.1	-66	29	8	3	0.934	0.190	-	-	*	N	
TRM092	5	24	52.3	-66	29	40	3	0.168	0.158	2.67	14.1	*	Y	S_{100}, S_{60}
TRM093	5	32	30.7	-66	29	30	3	0.831	3.085	50.70	-	*	Y	$S_{25} \gg S_{12}, S_{60}$
TRM094	5	32	8.7	-66	26	28	3	0.269	1.650	-	-	*	Y	$S_{25} \gg S_{12}, S_{100}(c), S_{60}(c)$
TRM095	5	27	15.7	-66	24	45	3	0.247	0.292	-	-	*	Y	NSO
TRM096	5	26	52.2	-66	23	29	1	0.116	0.084	-	-		N	
TRM097	5	35	3.6	-66	20	23	3	0.157	0.165	2.83	13.2	*	Y	S_{100}, S_{60}
TRM098	5	36	20.8	-66	19	22	3	1.840	0.429	-	-	*	N	
TRM099	5	28	59.5	-66	17	46	3	0.133	0.367	-	-		N	
TRM100	5	11	4.1	-66	16	54	3	0.171	0.301	-	-		N	
TRM101	5	31	41.7	-66	5	54	3	0.361	0.348	-	-	*	N	
TRM102	5	35	38.5	-66	3	54	3	0.266	1.760	21.50	53.5	*	Y	S_{100}, S_{60}
TRM103	5	29	52.2	-65	52	23	1	0.138	0.229	-	-		N	
TRM104	5	32	25.8	-65	51	22	3	5.545	1.168	0.23	-	*	N	
TRM105	5	21	34.9	-65	47	54	3	0.183	-	-	-	*	N	
TRM106	5	25	46.0	-65	46	55	3	0.716	0.168	-	-	*	N	
TRM107	5	22	10.9	-65	46	1	3	0.322	0.252	4.42	16.7	*	Y	S_{100}, S_{60}
TRM108	5	23	35.5	-65	44	51	3	0.322	0.180	-	-	*	N	
TRM109	5	22	38.6	-65	44	47	3	0.168	0.205	3.96	-	*	Y	S_{60}
TRM110	5	15	22.5	-65	36	47	1	4.072	1.688	-	-	*	N	
TRM111	5	25	5.8	-67	56	29	2	0.116	-	-	-	*	N	
TRM112	5	32	4.4	-67	44	21	2	0.821	-	-	-	*	N	
TRM113	5	4	54.3	-67	36	6	2	0.134	0.133	-	-	*	Y	$S_{60}(u)$

TABLE 3—Continued

Source	α			δ			Scan	$S_{12}(Jy)$	$S_{25}(Jy)$	$S_{60}(Jy)$	$S_{100}(Jy)$	PSC	Rej	Comments on Rejection
TRM114	5	28	48.0	-67	31	22	2	0.117	0.185	-	-		N	
TRM115	5	27	18.1	-67	31	20	2	0.178	-	-	-	*	Y	$S_{100}(u), S_{60}(u)$
TRM116	5	14	2.4	-67	30	34	2	1.310	8.330	56.40	-	*	Y	S_{60}
TRM117	5	3	52.8	-67	24	48	2	0.304	0.695	-	-	*	Y	$H\alpha$
TRM118	5	14	3.9	-67	26	31	2	0.403	4.250	12.40	-	*	Y	S_{60}
TRM119	5	3	49.7	-67	22	41	2	0.682	2.500	-	-	*	Y	$S_{100}(c), S_{60}(c)$
TRM120	5	25	59.1	-67	12	52	3	0.169	0.186	5.63	26.1	*	Y	S_{100}, S_{60}
TRM121	5	13	50.8	-67	10	38	2	0.169	0.248	6.20	26.5	*	Y	S_{100}, S_{60}
TRM122	5	4	39.9	-66	44	31	2	0.398	1.770	14.90	28.7	*	Y	S_{100}, S_{60}
TRM123	5	4	57.7	-66	42	34	2	0.160	0.281	-	-	*	Y	NSO
TRM124	5	37	14.2	-66	28	46	3	0.345	0.547	8.81	-	*	Y	$S_{100}(c), S_{60}$
TRM125	5	37	1.4	-66	24	3	3	0.192	0.368	6.87	-	*	Y	S_{60}
TRM126	5	23	4.0	-66	25	38	3	0.187	0.481	4.17	-	*	Y	S_{60}
TRM127	5	25	35.9	-66	17	23	2	0.794	-	52.20	74.3	*	Y	S_{100}, S_{60}
TRM128	5	25	1.3	-66	14	57	2	0.148	-	-	-		N	
TRM129	5	26	1.6	-66	14	53	2	0.305	0.227	-	-		N	
TRM130	5	21	15.6	-66	6	54	3	0.119	0.545	4.18	-	*	Y	S_{60}
TRM131	5	33	28.6	-66	4	23	3	0.188	0.219	3.66	-	*	Y	S_{60}
TRM132	5	36	18.8	-66	0	53	2	0.134	-	2.85	7.9	*	Y	S_{100}, S_{60}
TRM133	5	7	51.3	-65	42	27	2	0.166	0.221	-	-		N	
TRM134	5	5	26.2	-67	39	8	1	-	0.182	-	-	*	Y	$S_{100}(u), S_{60}(u)$
TRM135	5	43	17.2	-67	28	12	1	-	0.117	-	-		N	
TRM136	5	34	14.0	-67	27	12	3	-	0.407	-	-	*	Y	$H\alpha, NSO$
TRM137	5	3	9.6	-67	18	40	3	-	0.113	-	-	*	Y	$S_{60}(u)$
TRM138	5	31	0.8	-67	21	51	1	-	0.449	2.60	10.1	*	Y	S_{100}, S_{60}
TRM139	5	10	29.6	-67	12	36	3	-	0.163	2.79	-	*	Y	$S_{100}(c), S_{60}$
TRM140	5	11	1.2	-67	11	10	3	-	0.186	-	-	*	Y	$H\alpha, NSO$
TRM141	5	24	30.8	-67	12	8	3	-	0.134	3.41	13.2	*	Y	S_{100}, S_{60}
TRM142	5	22	43.6	-67	10	26	3	-	0.197	-	-	*	Y	$S_{100}(c), S_{60}(c)$
TRM143	5	21	35.7	-67	2	48	1	-	0.078	-	-	*	Y	PN
TRM145	5	36	8.8	-66	36	39	3	-	0.097	2.27	-	*	Y	S_{60}
TRM146	5	24	7.4	-66	32	25	1	-	0.083	0.52	-	*	Y	S_{60}
TRM147	5	18	3.9	-66	24	43	3	-	0.147	-	-	*	Y	1
TRM148	5	40	29.2	-66	19	25	3	-	0.335	-	-	*	Y	PN
TRM149	5	33	46.2	-66	17	31	3	-	0.154	-	-		N	
TRM150	5	34	38.7	-66	15	32	1	-	0.110	2.19	-	*	Y	$S_{100}(c), S_{60}$
TRM151	5	17	43.7	-66	4	58	3	-	0.262	0.84	-	*	Y	$S_{100}(c), S_{60}$
TRM152	5	25	15.3	-66	1	53	1	-	0.119	1.81	3.5	*	Y	S_{100}, S_{60}
TRM153	5	17	0.4	-66	2	33	3	-	0.379	2.98	-	*	Y	S_{60}
TRM154	5	32	16.6	-67	48	32	2	-	0.307	-	-	*	Y	NSO
TRM155	5	26	53.6	-67	41	52	2	-	0.367	1.90	-	*	Y	S_{60}
TRM156	5	14	16.5	-66	21	56	2	-	0.309	-	-		N	
TRM157	5	25	42.3	-66	20	16	2	-	0.498	-	-	*	Y	NSO
TRM158	5	25	51.6	-66	13	13	2	-	0.199	-	-	*	Y	$H\alpha$

NOTES.—TRM selected sources in the LMC north field. Fluxes listed in this table assume a flux distribution which varies as ν^{-1} (see § IV). Blank entries in the $S_{\nu}(12)$, $S_{\nu}(25)$, $S_{\nu}(60)$, or $S_{\nu}(100)$ columns imply either that no flux was detected at that wavelength, or that the region was so confused that the source extraction algorithm was unable to extract any flux, or that the flux density measurement is not reliable.

Key to individual columns is as follows:

Position: The right ascension and declination are given for equinox 1950.

Scan: Information on the scan directions in which each source was detected unambiguously is given. (1) Detected in EW scan; (2) detected in NS scan; (3) detected in both EW and NS scans.

PSC: Sources marked with a "*" have been associated positionally with an object in the IRAS PSC.

Rej: Designation of sources rejected as stellar candidates.

Comments on Rejection:

S_{100} : Source was rejected because it had $S_{\nu}(100) > S_{\nu}(60) > 2 S_{\nu}(25)$.

S_{60} : Source was rejected because it had $S_{\nu}(60) > 2 S_{\nu}(25)$.

$S_{25} \geq S_{12}$: Source was rejected because it had $S_{\nu}(25) > 4 S_{\nu}(12)$.

GC, C, NSO: Source was rejected because it coincided with a globular cluster, open cluster, or clearly nonstellar object on the V or I band Schmidt plates.

PN: Source was rejected because it coincided with a planetary nebula (Sanduleak refs).

H α : Source coincided with a knot of H α in the LMC emission-line survey of Davies, Elliott, and Meaburn 1976.

Of the 156 sources selected from LMC north field, 93 were subsequently rejected as AGB candidates. The following criteria were used to reject a source:

1. Objects having infrared emission characteristic of cold dust ($T \lesssim 200$ K), such as is commonly found associated with H II regions, star clusters, young star-forming regions, or background galaxies. As discussed in § IV, Galactic “cocooned” stars have their peak in infrared emission between 1 and 15 μm , and characteristic dust temperatures of $T \sim 400\text{--}1000$ K. All sources with $S_{\nu}(100) > S_{\nu}(60)$, $S_{\nu}(60) > 2 S_{\nu}(25)$, or $S_{\nu}(25) > 4 S_{\nu}(12)$ were rejected. Seventy-five sources were rejected as AGB candidates by this criteria.

By rejecting sources associated with 60 or 100 μm emission, and not selecting objects in highly confused regions, we bias our survey against AGB stars in, or near, star-forming regions. However, as we noted in § III, the typical age of an AGB star is at least 5×10^7 yr, providing sufficient time both for the star to drift a significant distance from the site of formation and for the H II region to dissipate. Thus, we do not expect our sample to be biased unduly by our inability to survey regions such as Shapley III.

2. Association with nonstellar objects present at *IRAS* position. If a globular cluster, open cluster, background galaxy, or H II knot was found within 50" of the *IRAS* position, it was assumed to be responsible for the infrared emission. In most cases where this was so, the source had already been rejected on the basis of its 60 or 100 μm emission. Twelve objects which were either heavily confused, or were undetected because they were below the instrumental sensitivity at longer wavelengths, was rejected on this basis.

3. Association with known planetary nebulae in the LMC. Four objects were found remaining which were identified with LMC planetary nebulae detected by emission-line grism surveys (Sanduleak, MacDonnel, and Davis Philip 1978; Sanduleak 1984). Planetary nebulae have been found to have characteristic *IRAS* flux distributions peaking at between 25 and 60 μm (Chester 1986). Because of *IRAS*'s lower sensitivity at 60 μm , the planetaries under discussion were usually only detected at 12 and 25 μm ; however, most exhibited $S_{\nu}(25) > S_{\nu}(12)$, as would be expected.

VI. OPTICAL IDENTIFICATION OF AGB CANDIDATES

Once these criteria had been applied, 63 sources remained with *IRAS* fluxes at 12 and 25 μm , characteristic of stellar photospheres or circumstellar dust shells (CDS). The identification of optical counterparts to these infrared sources was done using the *V*- and *I*-band survey of RM84. Three *V*- and five *I*-band UK Schmidt plates were scanned by the COSMOS measuring machine, providing size, shape, position, and magnitude data to a limiting magnitude of $I \sim 17$ and $V \sim 18$, although the data are incomplete for $I \gtrsim 16$ and for $V \gtrsim 17$. The calibration procedures used are described in detail in RM84. In summary, systematics limit the photometric accuracy to ~ 0.1 in *V* and *I*, and ~ 0.15 in $V - I$, with the positions quoted being accurate to $\sim 1''$.

Seventeen of the *IRAS* sources could easily be identified with bright foreground stars ($I \lesssim 9.0$). A number of these objects are SAO stars, or sufficiently bright to have been typed in the University of Michigan Spectral Catalog (Houk and Cowley 1975). The *V*-, *I*-, [12]-, and [25]-band magnitudes are shown for these objects in Table 4. (The magnitude scale for measurements in each *IRAS* band is defined in the Supplement. The zero points for 12 and 25 μm are given in the notes to Table 4.) It should be noted that the *I*-band magnitudes and $V - I$ colors quoted for bright stars have a systematic offset as a result of the inaccuracy of *I*-band calibration at $I \lesssim 8.0$.

In order to test whether these optical objects are feasible as the sources of the infrared flux detected by *IRAS*, PSC fluxes and *V*- and *I*-band photometry were determined for a sample of M giants, supergiants, and carbon stars. The giants and supergiants are from a sample of late stars taken by Lee (1970), and the carbon stars were selected from a sample taken by Mendoza and Johnson (1965). The Johnson photometry was converted to the Cousins system using the relations of Bessell (1979). Note that this conversion has only been measured for $V - I < 2.0$, although we have extended its application to larger $V - I$. The plot of $V - I$ versus $V - [12]$ color for these stars and the foreground stars in the TRM sample is shown in Figure 6a. Also included in Figure 6a is the locus of “normal” giant stars (i.e., giant stars without infrared excess) from K0 to M5 (Waters, Cote, and Aumann 1987). It can be seen that the untyped bright stars are consistent with being Galactic foreground dwarfs and giants.

Supergiants and giants clearly follow two different loci in this diagram, with supergiants having a larger infrared excess, presumably due to dust formation in their cool, extended envelopes. Carbon stars, which are of course on the AGB, would seem to occupy both the giant and supergiant regions. Carbon stars, with $V - [12]$ colors similar to those of the supergiants, must therefore have undergone significant mass loss while on the AGB in order to produce a dust shell responsible for the observed infrared excess.

The list of COSMOS optical sources was searched for all objects within 90" of the *IRAS* position in the cross-scan direction and 50" in the in-scan direction. For 17 of the *IRAS* sources, fairly bright counterparts in the range $11.0 > I > 9.0$ could be identified (see Table 4b). These objects are also plotted in Figure 6b—most fall in the region of the diagram occupied by M-type supergiants. Further, these objects are all too bright to be on the AGB in the LMC which has its tip at $I \sim 12\text{--}13$ (RMT87, Fig. 14). We have also shown in Table 4, where available, the rms standard deviation observed at *I* band (σ_I) for each star found to be significantly variable in the 23 epoch RGC study. The typical rms variation over all 23 plates was $\sigma_I \sim 0.06$, and well-defined periods can be determined only for $\sigma_I \gtrsim 0.2$. However, while the mean *I*-band magnitudes of these stars are well known, the *V* magnitudes are only known for three widely separated epochs. The quoted *V* magnitudes could, therefore, be uncertain by more than 0.5 mag, for a star variable at *I* band with $\sigma_I \gtrsim 0.2$.

Spectra have been obtained for most of these stars (see § VII

(c), (u): Source extraction algorithm was unable to produce a meaningful flux estimate at that wavelength, due to either (c) source confusion or (u) unselected source; however, it is clear from the *IRAS* maps that there is sufficient 60 μm or 100 μm flux present to reject the source.

1: TRM 147 showed some weak evidence for 60 μm flux which was not selected by the IPAC source extractor. Since this source had a PSC 60 μm flux greater than its 25 μm flux, it was therefore rejected.

The flux conditions were held to be stronger reasons for source rejection, so although a number of sources listed as being rejected on this basis were also coincident positionally with globular clusters, galaxies, etc., only the flux condition has been listed here.

TABLE 4
STELLAR AND CDS TRM SOURCES IN LMC NORTH

Source	[12]	[25]	[12-25]	α	δ	$d\alpha$	$d\delta$	V	I	V-I	V-[12]	V(kms ⁻¹)	Type	Src	ID or Comments
(a) Foreground Galactic Stars.															
TRM006	5.44	-	-	5 19 41.1	-67 55 41	0	21	10.20	7.71	2.49	4.76				3
TRM008	4.69	-	-	5 19 24.9	-67 54 47	4	14	9.74	6.99	2.75	5.05				3
TRM013	5.86	4.68	0.15	5 26 35.4	-67 51 54	-58	-76	9.67	8.52	1.15	3.81		G2V	M	HD 36347, ³
TRM019	1.06	0.42	0.37	5 43 55.1	-67 43 8	-6	20	8.99	3.54	5.45	7.93		M5/6III	M	HD 38941
TRM028	5.34	-	-	5 18 37.9	-67 35 33	3	-6	9.78	7.15	2.63	4.43				
TRM040	5.63	-	-	5 26 48.2	-67 26 58	1	-48	11.48	9.19	2.28	5.84				3
TRM048	4.22	3.48	0.33	5 4 15.5	-67 20 16	1	0	12.19	8.83	3.36	7.97				
TRM055	5.64	-	-	5 42 46.0	-67 9 33	-3	4	7.20	6.20	1.01	1.57		F7V	M	SAO 249339
TRM058	4.95	3.35	-0.02	5 32 36.7	-67 7 20	-21	78	9.37	8.30	1.07	4.42				3,4
				5 32 43.5	-67 7 2	17	97	17.26	13.84	3.42	12.31				⁵ $\sigma_I = 0.20$
TRM085	4.86	4.60	0.52	5 29 6.5	-66 43 28	-6	4	7.98	6.17	1.80	3.12		K0	S	SAO 249293
TRM090	5.77	-	-	5 19 46.9	-66 29 31	16	17	8.47	6.74	1.72	2.69				SAO 249253
TRM091	3.70	3.88	0.69	5 10 0.2	-66 29 2	-11	6	7.81	5.14	2.66	4.10		M4	S	SAO 249212
TRM098	2.97	2.99	0.63	5 36 20.0	-66 19 8	-4	15	8.68	5.19	3.49	5.72		M4III	S	SAO 249320
TRM104	1.77	1.90	0.68	5 32 26.0	-65 51 32	1	-10	9.38	4.88	4.50	7.61		M5/7III	M	HD37298
TRM106	3.99	4.01	0.63	5 25 46.4	-65 47 0	2	-5	7.84	5.64	2.21	3.85		K3/4III	M	HD 36316
TRM110	2.10	1.50	0.38	5 15 24.2	-65 35 52	10	56	11.00	6.05	4.95	8.89				3
TRM111	5.97	-	-	5 24 53.0	-67 56 24	-72	5	9.13	7.42	1.71	3.16		K1III	M	HD 36316, ³
(b) LMC Supergiants.															
TRM005	4.33	2.97	0.08	5 32 45.5	-67 57 10	-11	-7	13.48	10.61	2.87	9.15	218	M4I	O	HV 996, ⁵ $\sigma_I = 0.28$
TRM036	4.81	3.68	0.17	5 14 53.9	-67 30 37	11	2	12.55	9.88	2.66	7.74	309	M3I	O	HV 916, ⁵ $\sigma_I = 0.18$
TRM043	4.72	3.34	0.07	5 12 49.2	-67 23 4	7	36	13.45	9.93	3.53	8.73				HV 2360, ^{3,5} $\sigma_I = 0.29$
TRM046	4.58	3.62	0.24	5 30 26.0	-67 22 15	-6	-39	12.54	10.03	2.51	7.96				^{3,5} $\sigma_I = 0.27$, P $\sim 614^d$
TRM049	5.46	4.35	0.18	5 29 59.6	-67 20 47	2	-9	10.49	9.32	1.16	5.03				⁵ $\sigma_I = 0.17$, P $\sim 407^d$
TRM052	5.67	-	-	5 27 33.8	-67 16 35	2	53	11.96	10.24	1.72	6.29				^{3,5} $\sigma_I = 0.15$, P $\sim 400^d$
TRM062	5.94	4.29	-0.03	5 35 22.1	-67 4 7	-14	24	13.00	10.44	2.56	7.06	305	M2I	O	HV 2700, ⁵ $\sigma_I = 0.16$
TRM063	4.95	3.95	0.23	5 33 31.1	-67 6 9	4	1	10.74	8.83	1.91	5.79	309	M4I	O	1
TRM065	5.68	-	-	5 28 17.6	-67 1 11	12	-12	13.45	10.51	2.94	7.77	303	M3I	O	HV 5854, ⁵ $\sigma_I = 0.18$
TRM067	4.85	3.51	0.09	5 36 27.9	-66 57 21	-2	7	13.25	10.25	3.01	8.40	303	M3I	O	HV 1004, ⁵ $\sigma_I = 0.18$
TRM068	4.93	3.72	0.14	5 35 30.6	-66 57 49	-10	7	11.74	8.96	2.78	6.81	336	M3I	O	⁵ $\sigma_I = 0.14$
TRM069	5.46	4.11	0.08	5 29 36.7	-66 57 43	-5	-7	12.17	10.83	1.33	6.71	306	M3I	O	HV 2586, ^{1,5} $\sigma_I = 0.12$
TRM073	5.52	4.09	0.06	5 27 35.7	-66 55 52	-5	13	12.83	10.34	2.48	7.31	305	M2/3I	O	HV 963, ⁵ $\sigma_I = 0.20$
TRM078	5.05	3.86	0.15	5 33 8.8	-66 50 2	-9	19	14.18	10.58	3.60	9.13	325	M2	O	HV 12437, ⁵ $\sigma_I = 0.35$
TRM087	5.59	4.40	0.15	5 31 53.5	-66 42 46	-11	-18	12.45	9.85	2.60	6.86	301	M3/4I	O	^{1,5} $\sigma_I = 0.18$
TRM089	5.10	3.75	0.09	5 31 35.7	-66 32 11	-4	-1	12.39	9.52	2.88	7.30	302	M2I	O	⁵ $\sigma_I = 0.14$
TRM105	5.48	-	-	5 21 35.2	-65 47 44	2	10	9.28	8.01	1.27	3.80	324	M0/1I	O	1
(c) LMC AGB Candidates															
TRM007	5.69	-	-	5 5 17.4	-67 51 23	42	14	16.79	13.84	2.95	11.10				^{3,5} $\sigma_I = 0.17$
				5 5 6.5	-67 52 40	-19	-63	17.65	14.61	3.04	11.96				⁵ $\sigma_I = 0.25$, P $\sim 401^d$
				5 5 3.7	-67 51 35	-35	2	17.13	13.55	3.58	11.44				^{1,5} $\sigma_I = 0.15$
TRM023	5.52	3.04	-0.37	5 9 47.0	-67 39 31	-62	43	15.41	12.43	2.98	9.89	295	M5	O	^{2,5} $\sigma_I = 0.20$, P $\sim 226^d$
TRM024	5.07	3.99	0.19	5 11 24.3	-67 40 20	32	-14	17.01	14.12	2.88	11.93	287	M3	O	2
TRM037	6.07	-	-	5 26 16.6	-67 31 4	55	0	17.94	14.06	3.88	11.87				^{3,5} $\sigma_I = 0.22$, P $\sim 400^d$
TRM060	3.72	1.56	-0.24	5 32 54.4	-67 9 10	-9	-46	17.42	13.95	3.47	13.70				^{3,5} $\sigma_I = 0.22$, P $\sim 210^d$
TRM072	5.73	-	-	5 11 43.2	-66 54 43	15	0	13.38	11.98	1.40	7.65	342	C	O	^{2,5} $\sigma_I = 0.18$
				5 11 35.3	-66 54 9	-29	34	15.54	13.04	2.50	9.81	313	M6	O	^{2,5} $\sigma_I = 0.15$
TRM079	5.26	4.16	0.18	5 30 20.0	-66 51 25	82	9	16.05	13.80	2.26	10.79				⁵ $\sigma_I = 0.14$
				5 29 58.6	-66 52 38	-38	-65	13.18	11.13	2.04	7.92				
TRM088	5.60	-	-	5 20 20.0	-66 38 58	2	-4	16.21	13.61	2.60	10.61	301	C	O	^{2,5} $\sigma_I = 0.16$
TRM096	5.97	4.76	0.14	5 27 0.8	-66 24 6	48	-37	16.38	14.13	2.25	10.41				^{3,5} $\sigma_I = 0.21$, P $\sim 379^d$
				5 27 4.1	-66 23 48	67	-18	14.29	13.05	1.24	8.32				⁵ $\sigma_I = 0.21$
TRM101	4.73	3.22	0.02	5 31 43.1	-66 5 43	8	11	14.67	11.72	2.96	9.94	317	M6	O	^{2,5} $\sigma_I = 0.25$, P $\sim 489^d$
TRM108	4.86	3.93	0.25	5 23 35.7	-65 44 38	1	14	14.26	11.24	3.02	9.40	319	M3/4	O	^{2,5} $\sigma_I = 0.35$, P $\sim 327^d$
TRM128	5.70	-	-	5 24 52.5	-66 14 22	-49	36	17.29	14.02	3.28	11.59				1
				5 25 6.4	-66 15 39	29	-41	17.10	15.67	1.43	11.40				3

TABLE 4—Continued

Source	[12]	[25]	[12-25]	α	δ	$d\alpha$	$d\delta$	V	I	V-I	V-[12]	V(kms ⁻¹)	Type	Src	ID or Comments
TRM129	4.92	3.68	0.13	5 26	7.5 -66 14 38	33	16	14.51	11.15	3.36	9.59				³ $\sigma_I = 0.17$
(d) Unidentified Objects.															
TRM004	4.57	3.42	0.16	5 11	28.6 -67 55 56	62	-5	18.05	16.10	1.94	13.48				
				5 11	28.4 -67 56 37	61	-46	17.46	15.69	1.77	12.89				
TRM009	5.65	3.37	-0.29	5 7	21.9 -67 52 38	-1	15	16.65	14.71	1.94	11.00				
				5 7	17.7 -67 53 38	-24	-45	17.03	15.13	1.90	11.37				
				5 7	25.5 -67 52 12	19	41	17.01	15.48	1.53	11.35				
				5 7	16.1 -67 52 38	-33	14	16.79	15.37	1.43	11.14				
				5 7	18.6 -67 52 36	-19	17	16.97	15.67	1.30	11.32				
TRM016	5.49	3.51	-0.17	5 24	12.9 -67 47 55	-20	25	16.80	15.53	1.27	11.30				
				5 24	22.1 -67 47 4	32	76	16.95	15.30	1.65	11.46				
				5 24	17.1 -67 49 50	4	-89	16.82	15.25	1.57	11.33				
TRM020	4.81	3.68	0.18	5 19	10.4 -67 48 55	37	-51	17.16	15.03	2.13	12.35				
				5 19	6.5 -67 47 53	15	11	17.14	15.56	1.58	12.33				
				5 19	4.7 -67 47 25	4	39	17.57	16.05	1.52	12.76				
TRM045	5.81	-	-	5 28	30.6 -67 22 50	52	24	16.87	15.29	1.58	11.06				³
				5 28	14.8 -67 22 17	-36	57	16.49	14.68	1.81	10.68				
TRM051	6.02	-	-	5 3	27.8 -67 15 4	-33	8	12.81	11.81	1.00	6.79				³
TRM077	5.25	4.12	0.17	5 36	6.7 -66 48 44	12	-13	14.83	13.48	1.35	9.57				⁵ $\sigma_I = 0.17$
TRM099	5.82	3.16	-0.44	5 29	1.7 -66 17 42	12	5	15.41	13.65	1.76	9.59				⁵ $\sigma_I = 0.25$
				5 28	59.6 -66 17 44	1	3	17.46	16.06	1.40	11.64				
TRM100	5.55	3.37	-0.25	5 11	4.9 -66 16 27	4	28	16.42	14.46	1.96	10.88				
				5 11	8.7 -66 16 33	26	22	16.44	14.94	1.50	10.89				
				5 11	8.2 -66 15 56	23	59	16.12	13.95	2.17	10.58				
TRM103	5.78	3.67	-0.22	5 29	53.7 -65 52 8	8	15	17.20	15.84	1.36	11.42				³
TRM112	3.84	-	-	5 32	11.7 -67 44 27	41	-6	13.22	11.74	1.48	9.37				^{3,5} $\sigma_I = 0.19$
TRM114	5.96	3.90	-0.20	5 28	48.3 -67 31 13	2	9	17.05	15.32	1.73	11.09				³
TRM133	5.58	3.71	-0.12	5 7	57.9 -65 42 40	37	-12	14.20	13.10	1.10	8.62				³
TRM135	-	4.40	-	5 43	17.2 -67 28 41	0	-28	13.78	12.26	1.52	13.78				³
TRM149	-	4.10	-	5 33	46.1 -66 16 45	0	46	15.30	13.56	1.74	15.30				⁵ $\sigma_I = 0.15$
TRM156	-	3.35	-	5 14	24.7 -66 21 48	47	9	16.47	15.08	1.39	16.47				³
				5 14	21.8 -66 21 22	30	34	17.17	15.99	1.18	17.17				
				5 14	10.4 -66 20 58	-34	59	16.85	15.22	1.63	16.85				
				5 14	23.8 -66 20 46	41	71	16.20	14.77	1.43	16.20				

NOTES.—Stellar and CDS TRM sources in the LMC north field. Optical positions and V - and I -band magnitudes presented are from the COSMOS scans of eight UK Schmidt plates in Reid and Mould 1984. Note that the I -band photometry is in the Cousins system.

Key to individual columns is as follows:

[12], [25]: Measured fluxes converted to the $IRAS$ magnitude scale as defined in the Supplement. Zero points used were 28.3 and 6.73 Jy at 12 and 25 μm , respectively.

[12-25]: $[12 - 25] = \log_{10}[S_{\nu}(12)/S_{\nu}(25)]$.

$d\alpha$, $d\delta$: $d\alpha = \alpha_{\text{COSMOS}} - \alpha_{\text{IRAS}}$ (in arcseconds), $d\delta = \delta_{\text{COSMOS}} - \delta_{\text{IRAS}}$ (in arcseconds).

V : Radial velocity measured as described in § V.

Type, Ref: Star type and luminosity class and Reference.

M: University of Michigan catalog of HD spectral types, Houk and Cowley 1975.

S: Smithsonian Astrophysical Observatory star catalog.

O: Typing based on spectral observations (see § V).

ID or Comments:

HD: Henry Draper catalog.

SAO: Smithsonian Astrophysical Observatory star catalog.

HV: Harvard variable catalog.

1. The image detected by COSMOS on the UKST plate was quite noncircular. Examination of the plate revealed a close or only partially resolved pair of stars. The magnitudes for such objects are uncertain by at least ± 0.3 .

2. Classified as an AGB star because this star is a carbon star, an M star which is too faint to be a supergiant, or of late spectral type and unlikely to be a supergiant.

3: $IRAS$ position is uncertain because the source was detected clearly in only one scan direction (see Table 3).

4. TRM 058 is probably a bright foreground star, although the AGB star listed could also be the optical counterpart.

5: RMS variation in I from the 23 photographic plates analyzed by RGC. This datum is given only for stars with significant variability. The typical rms variation is $\sigma_I \sim 0.06$. Period determinations are not well defined for $\sigma_I \lesssim 0.2$, since the uncertainty in individual data points is about ± 0.1 . Periods for the Harvard variables are given in RGC.

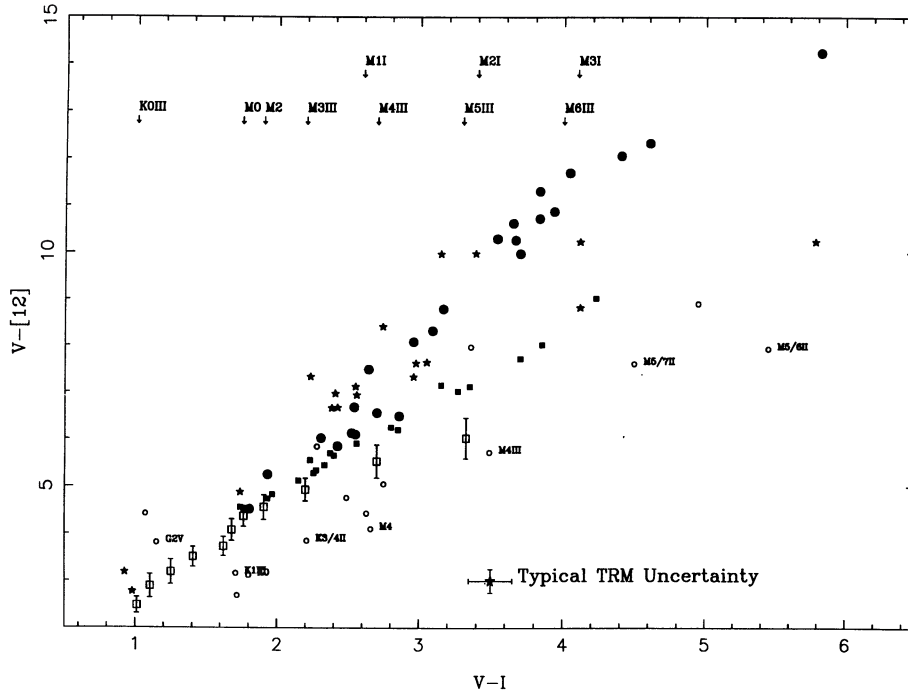


FIG. 6a

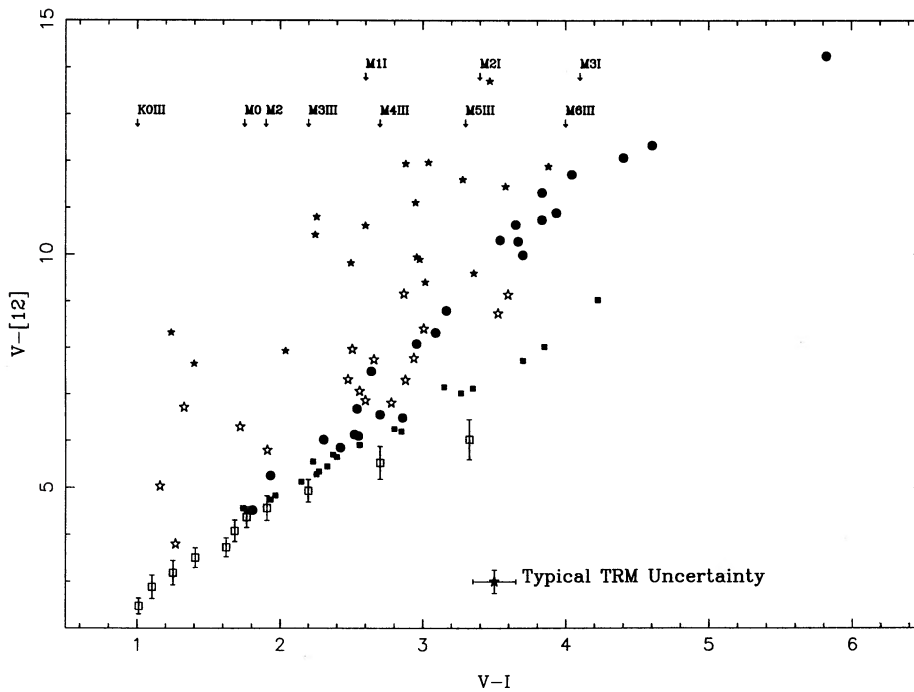


FIG. 6b

FIG. 6.—(a) $(V-I)/(V-[12])$ color-color diagram for Galactic supergiants (filled circles), giants (filled squares), and carbon stars (filled stars) (references in text), and TRM foreground objects (open circles). Boxes show the sequence of “normal” stars (i.e., stars without infrared excess) from K0 to M5, based on an analysis of the *IRAS* PSC by Waters, Cote, and Aumann (1987). Error bars represent the 1σ points in the spread of the relation. $V-I$ colors for representative spectral types are also shown. Most of the foreground stars are brighter than $I \sim 8$, and, with few calibrating standards our COSMOS-based photographic photometry is prone to systematic errors. These errors probably account for the offset relative to the standard sequence. (b) $(V-I)/(V-[12])$ color-color diagram for Galactic supergiants (filled circles) and giants (filled squares), as well as TRM supergiants (filled stars) and AGB candidates (filled stars) in the LMC. The sequence of “normal” stars is that plotted in (a). The typical photometric uncertainty for sources detected in our survey and shown in this diagram is $\sim \pm 0.15$ in $V-I$ and $\sim \pm 0.25$ in $V-[12]$. V -band magnitudes are, however, likely to be more poorly determined for variable stars (see text).

and Table 4), and all stars which were observed prove to be M stars, with radial velocities consistent with membership of the LMC. The few objects seen to lie above and to the left of the galactic supergiants in Fig. 6*b* are thought to have V magnitudes affected by variability, and, considering their measured σ_I (see Table 4), they are not inconsistent with being supergiants. Therefore, although not all these objects have been spectroscopically confirmed as M supergiants, their identification as such is reasonable.

Of the 31 remaining objects, at least 13 have red or optically variable candidates within the *IRAS* error box. These objects have colors consistent with being LMC AGB stars (also shown in Fig. 6*b* and listed in Table 4c). As noted, a few of these objects have been confirmed spectroscopically as being either C stars or late M-type stars. The remaining IR sources have been listed in Table 4d, along with all COSMOS counterparts within the *IRAS* error box having $V - I > 1.1$.

We have also listed the logarithm of the ratio between $S_{\nu}(12)$ and $S_{\nu}(25)$ (labeled [12–25] in Table 4) for all possible sources. It is expected that for stars with infrared emission primarily resulting from a photosphere, [12–25] will accumulate to a value ≈ 0.64 (Habing 1987). We find this to be true for about half of our foreground dwarf and giant stars. Stars with infrared emission from circumstellar dust, however, have been found to have characteristic values of $0.4 \gtrsim [12-25] \gtrsim -0.4$. The analysis of the PSC shows a very marked “gap” in the number of stars with $0.55 \gtrsim [12-25] \gtrsim -0.15$ (Habing 1987). However, it is just these colors that we observe in our samples of supergiants (which we know to have infrared excesses resulting from circumstellar dust), AGB candidates, and unidentified objects. Of the 31 objects in these groups for which we have 12 and 25 μm data, 30 satisfy the “dusty” color condition above—the mean values of [12–25] in each category are 0.12, 0.02, and -0.09 , respectively. In each class (and in particular for the AGB candidates and unidentified sources where we have uncertain optical identifications), these colors suggest a population of dusty stellar objects.

VI. SPECTROSCOPIC OBSERVATIONS

We have obtained intermediate resolution spectroscopic observations of the optically identified candidates using the modular spectrograph on the 2.5 m du Pont telescope at Las Campanas Observatory. This spectrograph is described in detail by Schechter (1988) and may be used in several different modes. Our observations were made using a cross-dispersed echellette configuration, with spectral coverage from ~ 4700 to ~ 9700 Å. The dispersion is ~ 70 km s $^{-1}$ per pixel in each of the 10 orders, and the resolution ranges from 1.7 to 2.5 pixels. The gratings used were a 100 line mm $^{-1}$ reflection grating and a 200 line mm $^{-1}$ transmission grating as cross-disperser. The latter is blazed at 6730 Å, and, as a consequence, the system is relatively insensitive shortward of 5000 Å. The detector is an 800 × 800 format Texas Instruments CCD with 15 μm pixels.

The observations were obtained during the eight nights from 1988 October 23/24 to 30/31. Conditions were clear and photometric on each night, with the seeing (as far as could be estimated from the TV guider) ranging from 1'0 to 1'5. Throughout the run, the slit width was set at 1'5, which, with the 85 mm camera lens used, projects to 1.8 pixels at the detector. The wavelength calibration was defined in the usual way using helium, neon, and argon arc lamps. Since our observations were confined within a restricted region of the LMC, calibration exposures were typically obtained after two-

three-program star observations. Cross-correlating the various arc spectra taken on a given night shows that the largest drift in the wavelength scale between successive calibration lamp exposures is only 0.2 pixels, or ~ 13 km s $^{-1}$. This is more than adequate to determine whether the stars are likely members of the LMC, the main purpose of the velocity measurements.

The data were reduced on the CIT astronomy department VAX 780 using standard FIGARO routines together with software written by J. McCarthy to deal with echelle reductions (McCarthy 1988). A number of the latter algorithms were modified by C. Steidel to allow for more accurate sky subtraction; optimal extraction (see Horne 1986) is possible with the (relatively) long slit Las Campanas modular spectrograph. After straightening the echelle orders and performing the extraction and sky subtraction, the data were wavelength calibrated and set on a flux scale using observations of the flux standard LTT 9239 (Stone and Baldwin 1983). The separate orders were then merged to give a one-dimensional spectrum. The spectral overlap between adjacent orders is large—typically 200 pixels—allowing one to check the relative accuracy of the flux calibration. Interorder adjustments of $\sim 3\%$ were typical, and, comparing our observations of Wolf 1346 and Hiltner 600 with the spectrophotometry by Oke (1974) and Stone (1977), respectively, the overall flux density calibration is accurate to $\sim 10\%$.

In the case of the observations of the *IRAS* sources, we adopted a position angle of the slit of 90° (east-west) in all cases; that is, we made no attempt to adjust to the parallactic angles. However, an RG 610 filter installed in the TV guider ensured that we were guiding at $\lambda_{\text{eff}} \sim 6500$ Å. All observations were obtained above an air mass of 1.32, so the maximum misalignment through atmospheric dispersion is $\sim 0''.4$ in the blue and only $\sim 0''.2$ in the red. This is likely to be comparable to the guiding errors.

We have determined radial velocities for our program stars using standard cross-correlation techniques. As templates, we used observations of the bright Galactic stars HD 189711 (C star), Vyssotsky 5 (M5 giant), and HR 7176 (K giant). Reducing the velocities to a heliocentric system, a comparison of our results with cataloged velocities for 21 stars indicates that the accuracy is ~ 19 km s $^{-1}$. We have estimated spectral types from a visual inspection of the spectra.

VIII. DISCUSSION

a) LMC Supergiants

We have identified most of the red giant LMC stars in Table 4 as supergiants, that is, young, (several $\times 10^6$ yr), massive ($m \gtrsim \sim 8 M_{\odot}$) stars which ignite carbon nondegenerately. We do so on the basis of the bolometric magnitudes we infer from the relation

$$M_{\text{bol}} = I - (m - M)_0 - A_I + BC_I,$$

where we have assumed a distance modulus of 18.4 for the LMC (Reid and Strugnell 1986) and a foreground absorption of $A_I = 0.175$ mag or $E_{B-V} = 0.1$. The bolometric corrections are calculated using the expression given in § II (see also the Appendix).

Nine of the probable LMC supergiants from our sample can be identified with known Harvard variables. All of these stars have *JHK*—and, in two cases, *L'*—photometry by WBF. Searching the *IRAS* PSC, we have found data for a further six supergiants from among the stars observed by WBF. All are

TABLE 5
LMC SUPERGIANTS

HV	$S_{2.2}$	S_{12}	S_{25}	R_{12}	M_{bol}	$M_{\text{bol}}^{\nu^2}$	$M_{\text{bol}}^{\nu^{-1}}$	\dot{M}
888	1.27	0.49	0.19	11.5	-9.08	-8.98	-9.06	3.8
894	0.44	0.22	0.18	14.8	-7.89	-7.73	...	3.6
916	0.65	0.30	0.18	14.0	-8.26	-8.11	-8.16	3.6
963	0.46	0.16	0.12	10.3	-7.86	-7.73	-7.67	2.4
996	0.66	0.47	0.35	21.7	-8.26	-8.03	-7.73	6.8
1004	0.66	0.29	0.21	13.4	-8.20	-8.04	-8.15	4.2
2255	0.69	0.37	0.31	16.1	-8.80	-8.69	...	6.1
2360	0.56	0.33	0.25	17.8	-8.10	-7.97	-8.74	4.9
2532	0.48	0.27	0.10	16.9	-7.97	-7.79	...	2.0
2586	0.28	0.16	0.12	16.7	-7.55	-7.39	-7.19	2.4
2700	0.34	0.11	0.10	9.4	-7.60	-7.48	-7.78	1.9
5854	0.39	0.14	0.05	10.4	-7.71	-7.59	-7.86	1.0
12437	0.28	0.24	0.15	26.0	-7.44	-7.20	-7.97	3.0
12420	0.42	0.37	0.17	26.5	-7.96	-7.74	...	3.3
12501	0.49	0.37	0.31	22.5	-8.15	-7.95	...	6.1

NOTES.—LMC supergiants from the Harvard variables catalog. The flux densities are given in janskys, with K -band measurements taken from Wood, Bessell, and Fox 1981 and the *IRAS* data either from Table 2 or from the *IRAS* PSC. HV 5854 has no 25 μm detection, and we have estimated S_{25} for this star. Color corrections of 0.9 and 0.8 have been applied to the *IRAS* 12 and 25 μm data. R_{12} is the ratio between the observed 12 μm flux density and that predicted by $S_{\nu} \propto \nu^2$. Bolometric magnitudes have been calculated by integrating the flux from the observed distribution (M_{bol}); by adopting $S_{\nu} \propto \nu^2$ longward of 2.2 μm ($M_{\text{bol}}^{\nu^2}$); and by using the $V-I$ colors ($M_{\text{bol}}^{\nu^{-1}}$). Finally, the mass loss estimated from Jura's 1987 formula, with $S_{\nu}(60)$ set at 0.5 $S_{\nu}(25)$, is given in units of $10^{-5} M_{\odot} \text{yr}^{-1}$.

outside the region studied in this paper, although HV 888 is within the boundaries of the RM84 photographic survey. Of these 15 stars, only HV 2360 was detected at 60 μm by *IRAS*, with the typical upper limits of $\lesssim 0.2$ Jy. *IRAS* data for all these stars, color corrected under the assumption of a correction factor of 0.9 at 12 μm and 0.8 at 25 μm , are presented in Table 5. These correction factors are appropriate for an object with a temperature of ~ 1000 K. Although some of the LMC stars may have cooler dust shells, the inaccuracies introduced by our using the given correction factors are less than 10%; in most cases, less than the uncertainties in the *IRAS* flux measurements. The corresponding uncertainty in the bolometric magnitude is less than 1%.

Although our observations of these variable stars were obtained at different epochs, we can construct relatively accurate flux density distributions for comparison with the Galactic counterparts of the LMC stars. For the stars in the LMC (north) field we can use the I -band magnitudes derived by Reid, Glass, and Catchpole (1987). (Note that HV 2586 is misidentified as HV 2578 in their Table 3b.) These data are based on photometry of up to 23 IVN UK Schmidt plates, and the mean magnitudes are accurate to $\sim \pm 0.1$. At V , we have at most three observations, and the typical amplitude of variation is over 1.5 mag—but only a few percent of the total energy is emitted at these wavelengths.

A more important region is the near-infrared, near the peak of energy distribution. WBF only obtained single *JHK* observations for several stars. However, although a few stars vary by as much as 0.4 mag at 2 μm (for example, HV 894), the typical amplitude of variation is less than 0.2 mag (as compared with 0.7–1.2 mag at 8000 \AA). Finally, Rowan-Robinson *et al.* (1986) found that most of the Galactic giants and supergiants in their sample were variable by $\sim 10\%$ at *IRAS* wavelengths. Thus, the uncertainties in the observations of the LMC stars exceed the likely amplitude of variation at far-infrared wavelengths.

Bearing these uncertainties in mind, Figure 7 plots the flux density distribution of the LMC supergiants. The visual and near-infrared broad-band data for HV 888 are taken from the simultaneous photometry presented in WBF's Table 5. Their I -band magnitude is 0.13 mag brighter than the mean value found by RGC; hence, the colors are likely to be representative of the star at mean light. Figure 8 shows a number of Galactic stars for comparison. The LMC stars can be divided into two groups on the basis of the shape of the flux distribution beyond 12 μm . All have excess radiation above that expected from a stellar photosphere at these wavelengths. Table 5 illustrates this, where we give the parameter, R_{12} , defined as the ratio between the observed flux at 12 μm and that predicted by extrapolating from the K -band photometry, assuming that $S_{\nu} \propto \nu^2$. The LMC stars have values of R_{12} ranging from ~ 10 –30, as compared with ~ 5 –10 for the average Galactic stars with similar optical colors.

The first group of LMC stars, which includes the majority of the sample, has a spectral distribution that is nearly flat in S_{ν} for $\lambda \geq 12$ μm . The remaining stars have 25 μm flux densities, S_{25} , that are approximately half the value of 12 μm . The latter group have properties similar to most of the Galactic M giants and supergiants discussed by Rowan-Robinson *et al.* (1986). Table 6 presents data for some of these stars. The *IRAS* observations of these last stars were modeled by dust shells composed of dirty silicate grains, with the hottest grains having temperatures of $T_1 \sim 1000$ K.

Relatively few Galactic giants in the Rowan-Robinson *et al.* sample have 25/12 μm flux ratios as close to unity as the LMC stars. Furthermore, these Galactic stars with $S_{\nu}(25)/S_{\nu}(12) \sim 1$, either in the Rowan-Robinson *et al.* sample, or among the OH/IR stars studied by Herman, Burger, and Penninx (1986), generally have optical and near-infrared colors that are much redder than the LMC stars. In part, this is a selection effect, since the LMC stars would not be detected at optical wavelengths were they similar to NV Aur, for example, with $V-K > 12$. Conversely, in stars with hotter dust shells, the *IRAS* bands fall beyond the longer wavelength peaks in the energy distribution, and only the most luminous supergiants with spectra of this type can be detected in the LMC.

TABLE 6
GALACTIC GIANT AND SUPERGIANT STARS

Star	$S_{2.2}$	S_{12}	S_{25}	R_{12}	m_{bol}	$m_{\text{bol}}^{\nu^2}$	References
<i>o</i> Cet	7190	4881	2661	20	0.03	0.20	1, 2
R Vir	61.5	17.5	6.15	8.5	4.87	5.00	1
SUMa	41.4	4.23	1.40	3.1	5.84	5.89	1
R Hya	5874	1590	586	8.1	0.47	0.54	1
R Dra	70.0	19.3	7.9	8.3	5.25	5.33	1
χ Cyg	3288	1688	459	15.4	1.19	1.36	1
R And	940	315	173	10	2.56	2.70	3
IK Tau	1540	4634	2378	90.3	1.69	2.24	3
VY CMa	1178	9919	6651	253	1.44	2.87	4
RW Cep	116	97.4	91.6	25	4.39	4.53	3
PZ Cas	264	373	398	44	3.73	4.09	3
NV Aur	61.4	227	274	111	4.75	5.61	5

NOTES.—Galactic AGB and supergiant stars with circumstellar dust shells spanning a range of far-infrared properties. The flux densities are given in janskys and R_{12} has the same meaning as in Table 5. The apparent bolometric magnitudes are calculated using the same techniques adopted for the LMC stars in Table 5.

REFERENCES.—(1) Mendoza and Johnson 1965. (2) Zhou *et al.* 1986. (3) Lee 1970. (4) Hyland *et al.* 1969. (5) Hyland *et al.* 1972.

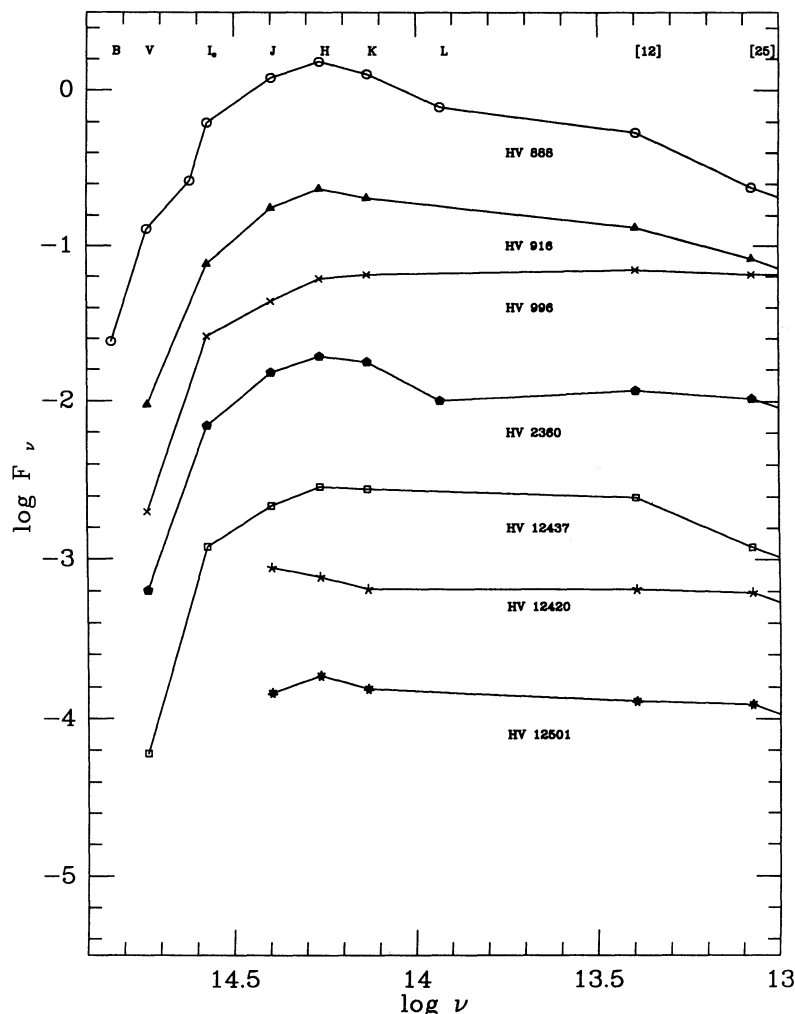


FIG. 7.—Flux density distribution of a representative sample of the Harvard variable supergiants listed in Table 5

Relatively flat flux density distributions at $\lambda > 12 \mu\text{m}$, comparable to those we observe in the LMC stars, can be attained in the Rowan-Robinson *et al.* models by increasing the optical depth at ultraviolet wavelengths ($\lambda < 4000 \text{ \AA}$) to $\tau_{UV} \geq 1$; by decreasing the ratio, r_1/r_2 , where r_1 is the inner and r_2 is the outer radius of the dust shell; or by decreasing the temperature, T_1 , of the hottest grains in the shell. Increasing τ_{UV} does not appear to be a viable option, because the LMC supergiants are not unduly red in $V-I$. Comparing the LMC supergiants with those observed by Rowan-Robinson *et al.*, the majority have characteristics which place them somewhere between PZ Cas and RW Cep, both of which were modeled by Rowan-Robinson and Harris (1982). The former star is an M3.5 supergiant with $M_{bol} \sim -8.3$ and a $(V-K)_0$ color of 5.8 mag, while RW Cep is a K5/M0 supergiant with $(V-K)_0$ of ~ 3.9 . (We have dereddened Lee's 1970 broad-band photometry using the interstellar reddening estimates made by Rowan-Robinson and Harris.) Both models have a grain condensation temperature, T_1 , of 500 K and $r_1/r_2 = 0.05$, with $\tau_{UV} = 0.5$ for RW Cep and $\tau_{UV} = 1.0$ in the case of PZ Cas.

WBF have calculated bolometric magnitudes for the Harvard variables from their near-infrared data, using a flux density distribution $S_\nu \propto \nu^2$ to extrapolate beyond $2.2 \mu\text{m}$. Obviously, this technique must underestimate the luminosity

of the stars in the current sample, which have infrared excesses. We have calculated bolometric magnitudes for these stars by integrating the flux density beneath the broad-band "spectra" plotted in Figure 6. We adopt a solar luminosity of $3.826 \times 10^{26} \text{ W}$ (Lang 1974) and an absolute magnitude of $M_{bol}(\odot) = 4.64$ (Buser and Kurucz 1978), as opposed to the value of 4.75 used by WBF. The zero points for the various passbands are taken from Berriman and Reid (1987), and the distance modulus of the LMC is taken to be 18.4 (WBF use 18.6).

Approximately 30% of the total flux emitted by the LMC stars originates at wavelengths beyond the K band. It is clear that the flux distribution falls to a minimum near $10 \mu\text{m}$, with radiation from the dust shell dominant at longer wavelengths. HV 2360 and HV 888 have L observations, which we have included in our calculations. Without these data, the calculated bolometric magnitudes for these two stars are brighter by 0.02 and 0.05 mag, respectively. However, for most stars we have no observations between K and the IRAS $12 \mu\text{m}$ data point, and we have simply integrated the flux using linear interpolation. Judging from the models calculated by Rowan-Robinson *et al.*, this approximation could lead to our overestimating the luminosity by $\sim 7\%$ at most.

What may be of equal importance is that this technique

takes no account of possible absorption between broad-band IJK data points. This is a significant problem among M dwarf stars, where strong steam bands can depress the spectrum more than 20% below the "continuum" as defined here (Berriman and Reid 1987). These water bands are weaker in M giants, but strong CO absorption bands occur. We have taken no account of the possible influence of these features. Thus, our results show the effect of adding the *IRAS* data for the bolometric scale defined by WBF. The true bolometric magnitudes may be a few tenths of a magnitude fainter than our present estimates. We have already discussed the uncertainties in combining the photometry from different epochs. For stars with no I -band or V -band data, we assume $I-J = 1.1$ and $V-I = 2.5$. Changing $I-J$ by 0.2 mag produces a difference of ~ 0.05 mag in the bolometric magnitude.

Our results are given in Table 5, where we also list the bolometric magnitudes derived under the assumption $S_\nu \propto \nu^2$ and magnitudes calculated from the $V-I$ colors. Typically, the former estimates are 0.1–0.2 mag fainter than the estimates based on the *IRAS* data. The magnitudes calculated from the $V-I$ data are in reasonable agreement with the (JHK, ν^2) calculations, except for the two reddest stars in the sample—

HV 2360 ($V-I = 3.53$) and HV 12437 ($V-I = 3.6$)—where the bolometric corrections are overestimated by over half a magnitude. The $V-I$ color for HV 12437 may be affected by variability, because our spectroscopic data indicate an earlier spectral type (WBF estimate M0.5) and an $R-I$ of ~ 1.0 , implying $V-I \sim 2$. Similarly, WBF assign a spectral type of M2 to HV 2360, rather than the M6+ that our $V-I$ estimate implies. Adopting $V-I = 2$ for both stars, the bolometric magnitudes become $M_{\text{bol}}^{V-I} = -8.15$ (HV 2360) and $M_{\text{bol}}^{V-I} = -7.5$ (HV 12437), closer to the other estimates.

Finally, we can make a rough estimate of the mass-loss rates from these stars. Jura (1987) has shown that mass-loss rates for carbon-rich and oxygen-rich stars in the solar neighborhood can be described by the relation

$$\dot{M} = 1.7 \times 10^{-7} v_{15} r^2 L^{-1/2} S_\nu(60) \lambda_{10}^{1/2} M_\odot \text{ yr}^{-1},$$

where v_{15} is the outflow velocity in units of 15 km s^{-1} , λ_{10} is the average wavelength of the flux distribution in units of $10 \mu\text{m}$, r is the distance in kiloparsecs, and L is the luminosity in units of $10^4 L_\odot$. We set both v_{15} and λ_{10} equal to 1. Only HV 2360 is detected at $60 \mu\text{m}$. However, observations of Galactic stars show that $S_\nu(60)$ typically lies in the range 0.75

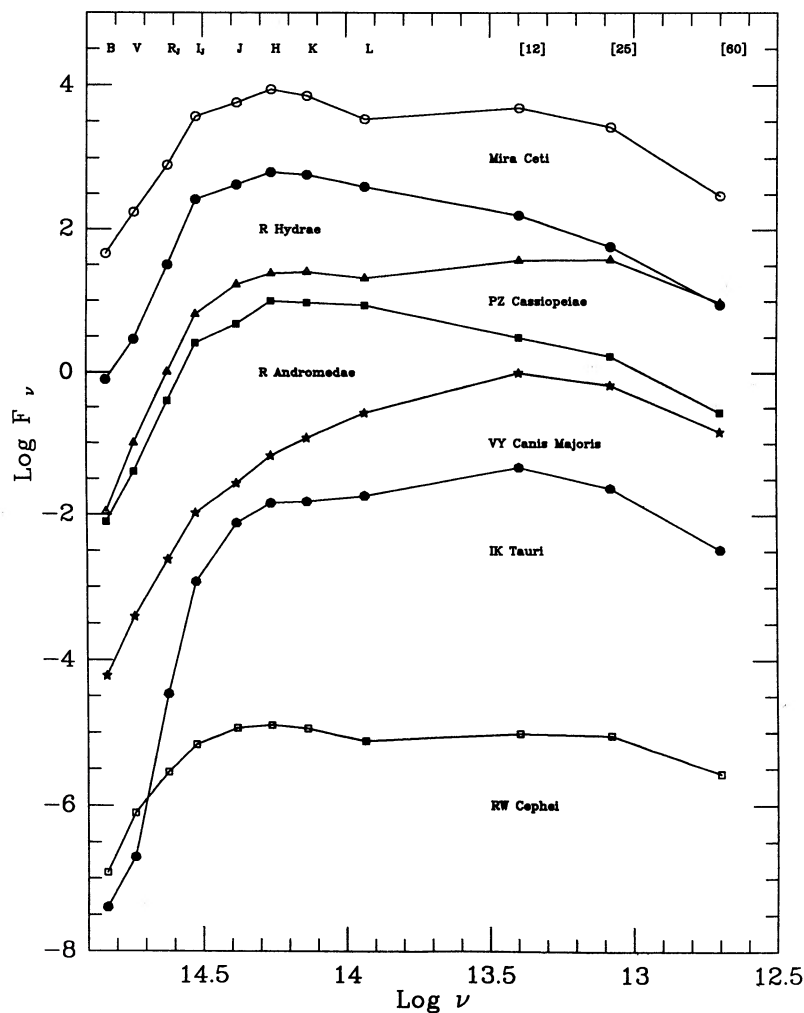


FIG. 8.—Flux density distribution of a representative sample of Galactic supergiants and AGB stars with circumstellar dust shells. Objects range from normal Mira variables (R And and \circ Cet) to the extreme supergiant VY CMa and the highly obscured AGB star IK Tau.

$\times S_v(25) \geq S_v(60) \geq 0.25 \times S_v(25)$, and we have assumed that $S_v(60) = 0.5 \times S_v(25)$ for the LMC stars. The implied mass-loss rates are several $\times 10^{-5} M_\odot \text{ yr}^{-1}$ —toward the upper end of the range exhibited by Galactic supergiant stars (Dupree 1986), but not particularly extreme.

b) *Optically Unidentified IRAS Sources*

Fifteen of the sources in Table 4 have been classed as optically “unidentified.” All, apart from the three objects detected only at $25 \mu\text{m}$, have [25-12] colors consistent with their being stellar, (Habing 1987) but there is neither a bright star nor an object with particularly red $V-I$ colors among the optically visible candidates. All could be heavily obscured AGB stars comparable to IRC +10216 or IK Tau. However, only TRM 112, which is not detected at $25 \mu\text{m}$, is brighter than 0.5 Jy at $12 \mu\text{m}$, and most have flux densities $S_v(12) < 0.20$ Jy. Comparing these observed values with the templates listed in Table 2, it is evident that if these unidentified sources are AGB stars, their luminosity does not exceed $M_{\text{bol}} \sim -6.0$. Infrared imaging is required to determine unambiguously the nature of these objects.

Using the available data, Table 4 lists the brightest objects visible on the I band plates that lie within the *IRAS* positional error box. Most have a $V-I$ color (on the Cousins system) of 1–2 mag, implying $V-[12]$ colors of 11 or more and $I-[12] > 10$. In comparison, PZ Cas, with $I_c - [12] \sim 7.4$, has $V-I_c \sim 4$, while RW Cep, which has a $V-I_c$ of 2.4, comparable with the redder stars in Table 4D, has an $I_c - [12]$ color of only 5.2. Even IK Tau ($V-I_c \sim 11$) has an $I_c - [12]$ of 9.3. Given these data, the majority of the listed objects are most unlikely to be associated with the *IRAS* sources.

There are a few possible exceptions to the last statement. The *IRAS* source TRM 051 lies within $35''$ of a 13th magnitude star for which we measure a $V-I_c$ color of 1.0. However, the data from our 23 I -band plates suggest that the star may be variable, although only at a relatively low level ($\sigma_I = 0.13$ mag), so we are unable to detect any possible periodicity. Hence, it is possible that our $V-I$ color is too blue and the star is either a supergiant or, less probably, a luminous AGB star.

TRM 099 has excellent positional agreement with a 16th magnitude stellar object with moderately blue colors. This star is definitely variable, with $\langle I \rangle = 15.80$ and $\sigma_I = 0.25$ mag from the 23 plate series. However, the three V band measurements agree to within 0.2 mag, and, despite the relative large amplitude, we can find no evidence for periodic variations. The $I_c - [12]$ color is nearly 10 mag, which again is difficult to square with the blue color at optical wavelengths.

Finally, the last three objects in Table 4d are detected by *IRAS* only in the $25 \mu\text{m}$ passband. It is possible that these are AGB stars with energy distributions similar to OH 20.7+0.1 (see Table 2), although one would probably expect a detection at $60 \mu\text{m}$. If so, TRM 156 is the most luminous, with $M_{\text{bol}} \sim -6.5$; with other two objects are nearly a magnitude fainter. An alternative, and more likely, explanation is that these objects are previously unobserved LMC planetary nebulae. As Table 2 shows, the flux density distribution of these objects peaks at $25 \mu\text{m}$. Further observations at near-infrared wavelengths are required to determine the nature of these objects, but it is unlikely that any are luminous AGB stars.

c) *The Candidate AGB Stars*

In Table 4c, we have listed those *IRAS* sources which may be associated with visible AGB stars in the LMC. In compiling

this list, we have included all sources where the $90'' \times 90''$ error box, centered on the *IRAS* position, embraces a star redder than $V-I = 1.5$ and with $11 \leq I \leq 15$. (Note that the C-star candidate for the TRM 072 is actually bluer than this limit. We observed this AGB star simply because it was the brightest star in the area.) This is clearly a liberal criterion, and many of the observed positional coincidences may have arisen by chance. Ideally, given the point-spread function appropriate to the *IRAS* detectors, we could calculate the probability that the AGB stars listed are associated with the *IRAS* detections. However, the situation is complicated by two factors; first, some of the objects were detected only in one set of *IRAS* cross scans, and have substantially larger positional uncertainties in one coordinate; second, the accuracy of the positional determination from the point-source filtering depends to some extent on the intensity above the local background. Thus, while the average positional residual for the LMC supergiants detected by both EW and NS scans is only $13''.0 \pm 7''.1$, one star (TRM 062) has an *IRAS* position that is offset by $28''$. On the other hand, those stars detected on only one scan have residuals of up to $\sim 50''$ in the other direction.

Seven of the sources in Table 4c have both EW and NS *IRAS* detections: TRM 023, 24, 72 (two stars), 79 (two stars), 88, 101, and 108. Of the nine stellar candidates, three—23 and 79 (both stars)—have positional residuals of more than $70''$ and are very unlikely identifications; two are marginal—the fainter star near TRM 072 ($r \sim 44''$) and TRM 024 ($r \sim 35''$)—and the four remaining stars (TRM 072 [brighter star], 88, 101, and 108) are plausible optical identifications.

Of the other sources, TRM 007 was detected only in the EW scans, and the second (and fainter) AGB candidate is positionally consistent with the *IRAS* source. Similarly, TRM 060 has a position that is consistent with the optically visible AGB star, and TRM 129—detected only NS—could also have an optical counterpart. The other *IRAS* sources—TRM 037, 96, and 128—show large positional residuals in the in-scan, as well as cross-scan, directions relative to the mooted optical counterparts.

The *IRAS* error boxes are large, so one also must take into account the local number density of AGB stars. As another means of assessing the likelihood of the listed objects being the *IRAS* sources, we have calculated the number density of AGB stars (using criteria given above) within a radius of $5'$ of each source. Table 7 presents these data for magnitude limits of $I \leq 12$ (N_{12}), $I \leq 13.1$ (N_{13}), $I \leq 14.25$ (N_{14}), and $I \leq 15$. Taking the surface density appropriate to the candidate and the observed displacement

$$r_1 = \sqrt{d\alpha^2 + d\delta^2},$$

we have calculated the “probability” (P) of finding a star of that magnitude or brighter within a displacement of $r \leq r_1$. This does not take into account the uncertainties in the *IRAS* position. From the LMC supergiants with data from both *IRAS* cross-scans, the agreement is generally better than $15''$, so we have adopted $r_1 = 15''$ for the AGB stars with small displacements.

Our results arrive at essentially the same conclusions as one draws from a visual inspection of Table 4c; the closer the positional coincidence, the more likely the association between optical and infrared. Typically, there are 12–15 AGB stars brighter than 15th magnitude within the $5'$ search radius, and the probability of a chance coincidence is 25% to 50%. Note, however, that most of the stars listed in Table 4c are redder

TABLE 7
SURFACE DENSITIES OF AGB STARS NEAR *IRAS* SOURCES

Star	N_{12}	N_{13}	N_{14}	N_{15}	I	r_1	P	M_{bol}^{V-I}
TRM 007.....	...	3	14	34	{ 13.84 14.61 13.55	{ 44.3 65.8 35.1	{ 0.31 1.63 0.19	{ -4.5 -3.8 -4.9
TRM 023.....	...	1	12	33	12.43	75.5	0.06	-6.0
TRM 024.....	...	1	15	37	14.12	34.5	0.20	-4.2
TRM 037.....	1	3	12	29	14.06	54.7	0.40	-4.3
TRM 060.....	3	4	10	16	13.95	47.6	0.25	-4.5
TRM 072.....	1	2	11	24	{ 11.98 13.04	{ 15.0 44.1	{ 0.003 0.24	{ -5.7 -5.2
TRM 079.....	4	4	11	22	{ 13.80 11.13	{ 82.2 75.7	{ 0.82 0.25	{ -4.3 -7.0
TRM 088.....	...	1	8	16	13.61	5.2	0.02*	-4.9
TRM 096.....	1	5	11	20	14.13	61.3	0.45	-5.1
TRM 101.....	1	1	10	16	11.72	13.3	0.002*	-6.6
TRM 108.....	1	1	5	18	11.24	13.5	0.002*	-6.8
TRM 128.....	2	5	12	17	14.02	60.8	0.49	-4.5
TRM 129.....	4	8	16	25	11.15	36.4	0.058	-7.3

NOTES.— N_{12} , N_{13} , N_{14} , and N_{15} give the number of AGB stars (defined as $I > 11$, $V - I > 1.5$) brighter than $I = 12$, 13.1, 14.25, and 15, respectively, and within a circle of radius $5'$ centered on the *IRAS* position. The I magnitudes and displacement (r_1) of the candidates listed in Table 4c are listed, and P gives an estimate of the probability of an AGB star of that magnitude or brighter being found at $r \leq r_1$. For those objects marked *, we have, following the arguments outlined in the text, set r_1 to $15''$ before calculating P . Bolometric magnitudes were calculated using the $V - I$ color, setting $BC_I = 0.18$ for $V - I > 3.0$ and assuming $E_{V-I} = 0.125$ mag. Based on our spectroscopic observations, we have taken $V - I$ to be 2.0 for TRM 108.

than $V - I = 2.5$. These lower temperature stars are rare, and it is possible that, by using the surface density of all AGB stars, we are underestimating the probability of their being *IRAS* sources. Nonetheless, we are again left with four good candidates—TRM 072, TRM 088, TRM 101, and TRM 108—while TRM 129 is a borderline case. We have spectra of each of the four best candidates, which we plot in Figure 9, while bolometric magnitudes (estimated from the $V - I$ colors) are given in Table 7. None show spectral peculiarities, but the optical spectra of the LMC supergiants with dust shells are similarly unremarkable.

Consider these five candidates separately:

1. *TRM 072*.—The associated carbon star has relatively blue colors, confirmed by our spectroscopy which indicates an $R - I$ of ~ 0.7 . The star is number 106 in the Westerlund *et al.* (1978) objective prism survey, which found many similarly hot C stars. The star is also among the brighter LMC carbon stars with a bolometric magnitude of -5.7 [for this star and TRM 088, we have calculated the bolometric correction BC_I using

$$BC_I = 1.9 - 0.7(V - I),$$

as described in Reid and Mould 1985; see also the Appendix to this paper.] There is no detection at $25 \mu\text{m}$, but if we assume $S_{\nu}(60) \sim 0.25 S_{\nu}(12)$, we find a mass-loss rate of $\sim 1.3 \times 10^{-5} M_{\odot} \text{yr}^{-1}$.

2. *TRM 088*.—The proposed optical counterpart is more like the typical LMC C star, with red $V - I$ colors and a bolometric magnitude near -5 . Again, there is no $25 \mu\text{m}$ detection—the $12 \mu\text{m}$ flux is only 0.16 Jy—but if we assume $S_{\nu}(60) \sim 0.04 \text{ Jy}$, $\dot{M} \sim 2 \times 10^{-5} M_{\odot} \text{yr}^{-1}$.

3. *TRM 101*.—Our spectrum shows this to be a late-type M giant. The star is variable, with sufficient amplitude to allow us to estimate the period. Plotting TRM 101 on the (M_{bol} , period) diagram (see RGC, Fig. 9), the position is constant with an AGB star of present-day mass $3-4 M_{\odot}$, while the bolometric

magnitude places the star on the upper AGB. We estimate the mass-loss rate as $\sim 4 \times 10^{-5} M_{\odot} \text{yr}^{-1}$.

4. *TRM 108*.—This star has properties reminiscent of HV 12437. The spectral type and spectroscopic $R - I$ color (~ 0.9

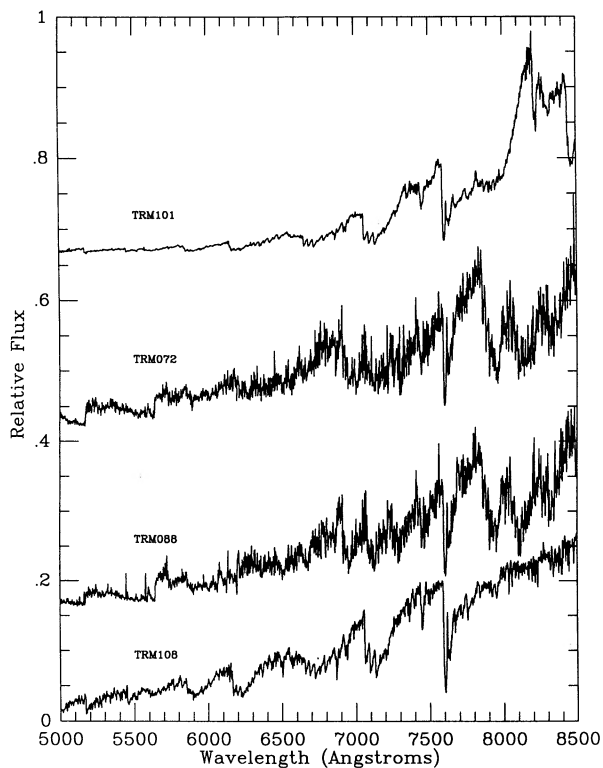


FIG. 9.—Spectra of the four AGB stars most likely to have been detected by *IRAS*.

mag) disagree with the photographic $V-I$ color, and again variability is the likely cause. Assuming that $V-I = 2$, we derive a bolometric magnitude of -6.8 which, with a period of 327 days, places the star near the $7 M_{\odot}$ supergiant track in the (M_{bol} , period) plane. Further observations at near-infrared wavelengths to check M_{bol} and in the optical region to confirm the period are required, but on balance this star is more likely to be a supergiant. The mass-loss rate, following our standard assumptions, is $\sim 2 \times 10^{-5} M_{\odot} \text{ yr}^{-1}$.

5. *TRM 129*.—Unfortunately, we have no spectrum of this star. The formal bolometric magnitude estimate places the star beyond the tip of the AGB—but only by 0.15 mag, somewhat less than the uncertainty in the estimate. If confirmed—there is evidence for variability—the red $V-I$ color is suggestive of an AGB star. We estimate the $60 \mu\text{m}$ flux density as 0.11 Jy, implying $\dot{M} \sim 2 \times 10^{-5} M_{\odot} \text{ yr}^{-1}$.

In summary, of the sources listed in Table 4c, five probably have optical counterparts, three of which are definitely AGB stars, while the other two may prove to be either luminous AGB stars or relatively low-luminosity supergiants. The mass-loss rates that we have inferred for these stars are considerably higher than the standard Reimers formalism would predict as appropriate for the calculated luminosities. Taking η as $\frac{1}{3}$, we expect $\dot{M} \sim 10^{-6} M_{\odot} \text{ yr}^{-1}$ at $M_{\text{bol}} = -6$. On the other hand, these mass-loss rates are similar to those derived by Knapp and Morris (1985) for AGB stars such as R Scl and V Hya, which have optically thick CO envelopes.

IX. CONCLUSIONS: THE COCOON STAR HYPOTHESIS

The main aim of our investigation is to test the hypothesis that a significant fraction of these stars evolving on the upper asymptotic giant branch ($M_{\text{bol}} < -6$) could be hidden from optical surveys by being enshrouded in dusty circumstellar envelopes. To explain fully the observed deficit, our *IRAS* analysis should have turned up several hundred sources with flux densities in the range $0.15 \leq (S_{\nu}[12], S_{\nu}[25]) \leq 0.6$ Jy. Clearly, these sources are not present in our sample. Ruling out this hypothesis—hiding the AGB stars—one is left with the option of removing the stars from the AGB before they attain $M_{\text{bol}} \sim -7.1$. Mass loss is the obvious mechanism, and our observations may give some support to the view that mass loss can curtail evolution along the AGB at an earlier level than previously supposed.

Apart from the three to five sources which we have identified with optically visible AGB stars, there remain 21 sources with no optical counterparts, but whose *IRAS* fluxes are consistent with those expected from the hot dust in circumstellar envelopes. (We exclude the three objects in Table 4d which were detected only at $25 \mu\text{m}$.) These may be “cocoon” stars, but, if so, the majority have luminosities fainter than $M_{\text{bol}} = -6$. Assuming that all are AGB stars, we can use the flux densities predicted for the $M_{\text{bol}} = -6.4$ templates (Table 2) to estimate their luminosity. Table 8 presents the results of this exercise, where we also note the templates used (we have averaged the predictions based on OH 32.0–0.5 and OH 20.7+0.1, which have similar energy distributions), and set a lower limit to the $I - [12]$ color assuming a limiting magnitude of $I = 18$ for the photographic plates.

The estimates made by this method obviously have large uncertainties; in some cases, we are using an observation at one wavelength to infer the complete spectral energy distribution. In most cases, the OH 32.0/20.7 composite

TABLE 8
THE UNIDENTIFIED SOURCES AS AGB STARS

TRM (1)	Template (2)	M_{bol} (3)	$I - [12]$ (4)	$S_{\nu}^p(60)$ (5)	$S_{\nu}^{\text{obs}}(60)$ (6)
4	IRC	-5.8	13.4
7	IRC	-4.7	12.3
9	32.0/20.7	-6.3	12.3	0.54	...
16	32.0/20.7	-6.5	12.5	0.60	<0.2
20	32.0/20.7	-7.1	13.2	1.15	<0.2
23	26.5	-5.4	12.5	0.13	~ 0.37
24	IRC	-5.4	12.9
37	IRC	-4.5	11.9
45	IRC	-4.8	12.2
51	IRC	-4.7	12.0
60	32.0/20.7	-8.2	14.3	3.11	$\leq 0.72(\text{c})$
77	IRC	-5.1	12.8
79	IRC	-5.1	12.7
96	IRC	-4.4	12.0
99	32.0/20.7	-6.1	12.2	0.44	~ 0.23
100	32.0/20.7	-6.4	12.5	0.58	<0.2
103	32.0/20.7	-6.2	12.2	0.47	c.
112	IRC	-6.4	14.2
114	32.0/20.7	-6.0	12.0	0.41	≤ 1.17
128	IRC	-4.7	12.3
133	32.0/20.7	-6.4	12.4	0.58	<0.2

NOTES.—Bolometric magnitudes predicted for the sources from Tables 4c and 4d without identified optical counterparts and assuming that all are enshrouded AGB stars. We give the lower limit to the $I - [12]$ color, based on an assumed detection limit of $I = 18$. The observed *IRAS* fluxes are matched against the template flux densities given in Table 2. Sources with $S_{\nu}(25) < S_{\nu}(12)$ are taken to be similar to IRC + 10216, while OH 26.5 is taken as appropriate if $S_{\nu}(12) \sim S_{\nu}(25) > S_{\nu}(60)$. For the remaining objects, we have averaged the predicted flux densities for OH 32.0 and OH 20.7 to give a composite template. In several cases, this last approximation predicts $60 \mu\text{m}$ flux densities which should have been detected in the present survey. Col. (5) lists the predicted flux density, in janskys, while col. (6) gives the observed value. The comment “c” denotes that the $60 \mu\text{m}$ map is confused, while an upper limit of 0.2 Jy indicates that no flux was detected above the noise level.

template, which we have assumed appropriate to sources with $[12-25] < \sim -0.2$, predicts a $60 \mu\text{m}$ flux density which should have resulted in a detection in the present investigation (note TRM 060 in particular). In such cases, the true energy distribution must fall off more rapidly than we have assumed, and our estimate of M_{bol} is too bright. Using OH 26.5 as the template for such stars reduces the inferred $60 \mu\text{m}$ flux, and the total luminosity of the source, by more than a factor of 2. Bearing this possible systematic error in mind, it is evident that most of the estimated bolometric magnitudes given in Table 8 lie in the range $-4.5 \leq M_{\text{bol}} \leq -6$.

What, then, can we deduce, given all our assumptions, about AGB evolution? If the mass-loss rates estimated in § VIIIc are reasonable, then the optically visible AGB/*IRAS* stars are losing mass about 10 times faster than is usual for AGB stars. We can speculate that these stars are moving toward the final superwind phase of evolution which precedes planetary nebula formation, and that the few we observe are the precursors of the optically unidentified *IRAS* sources. If so, the distribution of bolometric magnitudes in Table 8 implies that a planetary nebula ejection in $4-6 M_{\odot}$ stars can be triggered well below the tip of the AGB. Moreover, the mechanism is stochastic, since only some stars with initial masses in this range evolve to luminosities close to the theoretical limit, while others fail to reach $M_{\text{bol}} = -5.5$. We noted above that there are neither carbon stars among the luminous long-period variables—unambiguously AGB stars—nor among the nonvariable red

giants. This suggests that carbon-rich envelopes may be ejected at lower luminosities for a given stellar mass.

If we accept the assumption that all AGB stars pass through these two stages—dusty, but optically visible, and then enshrouded in a circumstellar shell—as part of the terminal phase of AGB evolution, we can use our observations of the number of stars in each stage to estimate lifetimes. There are approximately 370 AGB stars with $M_{bol} < -5.0$ in our optical surveys. Taking their average lifetime as $\sim 2 \times 10^6$ yr, we estimate average lifetimes of $\sim 3 \times 10^4$ yr for the optically visible *IRAS* sources (five stars), and $\sim 10^5$ yr for the enshrouded sources (15 objects). This last estimate, of course, will be too high if only a fraction of the unidentified sources prove to be AGB stars. It is also possible that the latter group may include

objects in transition between the two groups—objects with *V* magnitudes fainter than 20 (and invisible on the photographic plate), but *I* brighter than 18. Clearly, more accurate positions for the *IRAS* sources—using near-infrared imaging—are required.

These speculations need to be tested. However, the main conclusion of our investigation, that enshrouded cocoon stars can only form a minor constituent of the AGB population in the LMC, appears well founded, and is not affected by the nature of the optically unidentified objects.

The authors acknowledge useful discussions with M. Jura. This research was partly supported by an *IRAS* grant from NASA.

APPENDIX

JHK PHOTOMETRY OF LMC AGB STARS

Reid and Mould (1984, 1985) estimated bolometric magnitudes for LMC AGB stars from their *I*, *V* – *I* photometry. Frogel (1988) has warned, however, that this can lead to systematic errors with late-type stars. In 1987 January, we were able to carry out infrared photometry of three samples of these stars, using an InSb detector mounted at the Cassegrain focus of the du Pont 2.5 m telescope. We obtained the *JHK* photometry recorded in Table 9 on the CIT system of Elias *et al.* (1982). Bolometric magnitudes were then calculated following Frogel, Persson, and Cohen (1980) and assuming $E(J - K) = A_K = 0.02$.

The first sample is identified by Mould and Reid (1987) and is located in Shapley Constellation III. The mean difference between the *JHK* bolometric magnitudes and the *VI* bolometric magnitudes is 0.18 ± 0.06 , with a dispersion of 0.23 mag. Excluding X309

TABLE 9
A. INFRARED PHOTOMETRY

Number	<i>K</i>	<i>H</i> – <i>K</i>	<i>J</i> – <i>K</i>	m_{bol}	m_{bol}^{V-I}	Number	<i>K</i>	<i>H</i> – <i>K</i>	<i>J</i> – <i>K</i>	m_{bol}	m_{bol}^{V-I}
X114	11.51	0.24	1.13	14.48	14.36	A3	11.47	0.20	1.06	14.37	14.06
X116	10.08	0.14	0.82	12.49	12.51	A4	11.33	0.23	1.12	14.29	13.96
X124	10.18	0.16	0.91	12.78	12.76	A5	11.75	0.16	1.01	14.58	14.54
X149	11.12	0.28	1.14	14.10	13.86	A6	9.02	0.20	0.95	11.71	11.52
X162	9.53	0.18	0.88	12.06	12.11	A7	11.75	0.17	0.99	14.55	14.45
X245	7.44	0.30	0.95	10.13	10.31	A11	11.52	0.21	1.11	14.47	14.29
X274	11.45	0.22	1.07	14.36	14.16	A15	11.20	0.22	1.04	14.08	13.52
X275	9.43	0.19	0.92	12.05	12.00	A16	10.01	0.66	1.72	13.17	13.32
X285	9.29	0.18	0.86	11.78	11.58	A18	11.38	0.18	1.02	14.24	14.21
X286	8.94	0.20	0.92	11.56	11.48	A21	10.78	0.28	1.09	13.71	13.52
X309	9.43	0.21	0.96	12.14	11.48	A24	11.69	0.13	0.94	14.36	14.26
X317	8.92	0.20	0.97	11.67	11.43	A25	11.95	0.24	0.99	14.52	14.57
Z410	11.21	0.27	1.11	14.16	14.02	B63	10.28	0.68	1.76	13.46	13.61
Z438	10.97	0.43	1.35	13.91	14.26	B65	11.16	0.29	1.18	13.93	14.26
Z630	8.86	0.20	0.94	11.53	10.95	B71	10.28	0.43	1.38	13.25	13.61
Y879	11.70	0.27	1.07	14.61	14.26						
Y923	10.64	0.48	1.43	13.64	13.84						
Y943	10.18	0.57	1.60	13.28	13.62						

B. LUNDGREN STARS

Number	<i>K</i>	<i>H</i> – <i>K</i>	<i>J</i> – <i>K</i>	m_{bol}
S146	9.83	0.32	1.17	12.84
S167	9.17	0.22	1.12	12.13
S193	7.58	0.33	1.00	10.39
S186	8.98	0.28	1.12	11.94
S206	9.66	0.23	1.07	12.57
S281	7.78	0.43	1.36	10.95
S328	9.47	0.20	1.01	12.30
S362	9.63	0.24	1.09	12.56
G143	10.21	0.23	1.10	13.15
G159	9.47	0.32	1.17	12.48
G1999	11.37	0.19	1.04	14.25
G220	10.99	0.23	1.05	13.88
G278	9.84	0.26	1.17	12.85

and Z630, both of which have $V - I > 3$ but spectral types of K5, the mean difference is 0.11 with a dispersion of 0.14 mag. There is a systematic difference, however, for the three carbon stars in the sample (Z438, Y927, and Y943) of -0.3 mag.

The second sample is from Reid and Mould (1985) and is located in the field under examination here. For the noncarbon stars $\delta m_{\text{bol}}(JHK - VI) = 0.09 \pm 0.05$ with $\sigma = 0.23$ mag. For the carbon stars (A16 and B71), $\delta m_{\text{bol}} = -0.25$.

The third sample comes from work by Lundgren (1988) and is also located within the boundaries of the present field. For the Lundgren sample which has photometric and spectrophotometric VRI magnitudes $\delta m_{\text{bol}}(JHK - VI) = 0.18 \pm 0.09$ with a dispersion of 0.34 mag. There is a good correlation between δm_{bol} for individual stars with Lundgren's estimated individual A_V extinction. This would appear to be an unreliable way of estimating reddening.

REFERENCES

- Becker, S. 1982, *Ap. J.*, **260**, 695.
 Becker, S., Iben, I., and Tuggle, R. S. 1977, *Ap. J.*, **218**, 633.
 Beichman, C. A., Neugebauer, G., Habing, H. J., Clegg, P. E., and Chester, T. J. 1988, *IRAS Catalogs and Atlases*, Vol. 1, *The Explanatory Supplement to the IRAS Catalogs* (NASA RP-1190).
 Berriman, G., and Reid, I. N. 1987, *M.N.R.A.S.*, **227**, 315.
 Bessell, M. S. 1979, *Pub. A.S.P.*, **91**, 589.
 Bessell, M. S., and Wood, P. R. 1984, *Pub. A.S.P.*, **96**, 247.
 Blanco, V. M., McCarthy, M. F., and Blanco, B. 1980, *Ap. J.*, **242**, 938.
 Buser, R., and Kurucz, R. L. 1978, *Astr. Ap.*, **70**, 555.
 Castellani, V., Chieffi, A., Pulore, L., and Tornambe, A. 1985a, *Ap. J. (Letters)*, **294**, L31.
 ———. 1985b, *Ap. J.*, **296**, 204.
 Chester, T. 1986, in *Proc. 1st IRAS Conf., Light on Dark Matter*, ed. F. P. Israel (Dordrecht: Reidel), p. 240.
 Davies, R. D., Elliott, K. H., and Meaburn, J. 1976, *Mem. R.A.S.*, **81**, 89.
 Dupree, A. K. 1986, *Ann. Rev. Astr. Ap.*, **24**, 377.
 Elias, J. M., Frogel, J. A., Matthews, K., and Neugebauer, G. 1982, *A.J.*, **87**, 1029.
 Frogel, J. A. 1988, *Ann. Rev. Astr. Ap.*, **26**, 51.
 Frogel, J. A., and Blanco, V. M. 1983, *Ap. J. (Letters)*, **274**, L57.
 Frogel, J. A., Persson, S. E., and Cohen, J. L. 1980, *Ap. J.*, **239**, 495.
 Frogel, J. A., and Richer, H. B. 1983, *Ap. J.*, **275**, 84.
 Habing, H. J. 1987, in *IAU Symposium 122, Circumstellar Matter*, ed. I. Appenzeller and C. Jordan (Dordrecht: Reidel), p. 197.
 Herman, J., Burger, J. H., and Penninx, W. H. 1986, *Astr. Ap.*, **167**, 247.
 Herman, J., and Habing, H. J. 1985, *Astr. Ap. Suppl.*, **59**, 523.
 Horne, K. 1986, *Pub. A.S.P.*, **98**, 609.
 Houk, N., and Cowley, A. 1975, *Catalogue of Two-dimensional Spectral Types for the HD Stars* (Univ. Michigan Astr. Dept.).
 Hughes, S. M. G., and Wood, P. R. 1988, *Proc. Astr. Soc. Australia*, **7**, 147.
 Hyland, A. R., Becklin, E. E., Frogel, J. A., and Neugebauer, G. 1972, *Astr. Ap.*, **16**, 204.
 Hyland, A. R., Becklin, E. E., Neugebauer, G., and Wallerstein, G. 1969, *Ap. J.*, **158**, 619.
 Iben, I. 1981, *Ap. J.*, **246**, 278.
 Iben, I., and Renzini, A. 1982, *Ap. J. (Letters)*, **259**, L79.
 ———. 1983, *Ann. Rev. Astr. Ap.*, **21**, 271.
 Jura, M. 1987, *Ap. J.*, **313**, 743.
 Knapp, G. R., and Morris, M. 1985, *Ap. J.*, **292**, 640.
 Lang, K. R. 1974, *Astrophysical Formulae* (Berlin: Springer).
 Lattanzio, J. C. 1988, in *Proc. ACS Symposium Origin and Distribution of the Elements*, ed. G. J. Mathews (Singapore, World Scientific), p. 1.
 Leavitt, H. S. 1906, *Ann. Harvard Coll. Obs.*, **60**, 87.
 Le Bertre, T. 1987, *Astr. Ap.*, **176**, 107.
 Lee, T. A. 1970, *Ap. J.*, **162**, 217.
 Lundgren, K. 1988, *Astr. Ap.*, **200**, 85.
 McCarthy, J. 1988, Ph.D. thesis, California Institute of Technology.
 Mendoza, E. E., and Johnson, H. L. 1965, *Ap. J.*, **141**, 161.
 Mould, J. R., and Aaronson, M. 1986, *Ap. J.*, **303**, 10.
 Mould, J. R., and Reid, I. N. 1987, *Ap. J.*, **321**, 156.
 Oke, J. B. 1974, *Ap. J. Suppl.*, **27**, 21.
 Paczyński, B. 1970, *Acta Astr.*, **20**, 287.
 Payne-Gaposhkin, C. H. 1971, *Smithsonian Contr. Ap.*, **13**, 1.
 Reid, I. N., Glass, I. S., and Catchpole, R. 1987, *M.N.R.A.S.*, **232**, 53.
 Reid, I. N., and Mould, J. R. 1984, *Ap. J.*, **284**, 98.
 ———. 1985, *Ap. J.*, **299**, 236.
 Reid, I. N., Mould, J. R., and Thompson, I. 1987, *Ap. J.*, **323**, 433.
 Reid, I. N., and Strugnell, P. 1986, *M.N.R.A.S.*, **221**, 887.
 Reimers, D. 1975, in *Problems in Stellar Atmospheres and Envelopes*, ed. B. Baschek, W. H. Kegel, and G. Traving (Berlin: Springer), p. 229.
 Renzini, A. 1977, *Proc. Saas Fee Conf., Advanced Stages in Stellar Evolution* (Geneva: Geneva Obs.).
 Renzini, A., Bernazzini, M., Buonanno, R., and Corsi, C. E. 1985, *Ap. J. (Letters)*, **294**, L7.
 Rowan-Robinson, M., and Harris, S. 1982, *M.N.R.A.S.*, **200**, 197.
 Rowan-Robinson, M., Lock, T. D., Walker, D., and Harris, S. 1986, *M.N.R.A.S.*, **222**, 273.
 Sanduleak, N. 1984, in *IAU Symposium 108, The Structure and Evolution of the Magellanic Clouds*, ed. S. van den Bergh and K. S. de Boer (Dordrecht: Reidel), p. 231.
 Sanduleak, N., MacDonnel, B. J., and Davis Philip, A. G. 1978, *Pub. A.S.P.*, **90**, 621.
 Schechter, P. 1988, *A Guide to the Modular Spectrograph* (Carnegie Institute of Washington Observatories).
 Schwering, P. B. W. 1989, *Astr. Ap. Suppl.*, in press.
 Stone, R. P. S. 1977, *Ap. J.*, **218**, 767.
 Stone, R. P. S., and Baldwin, J. A. 1983, *M.N.R.A.S.*, **204**, 347.
 Waters, L. B. F. M., Cote, J., and Aumann, H. H. 1987, *Astr. Ap.*, **172**, 225.
 Wesselink, A. J. 1959, *M.N.R.A.S.*, **119**, 576.
 Westerlund, B. E., Olander, N., Richer, H. B., and Crabtree, D. R. 1978, *Astr. Ap.*, **31**, 61.
 Wood, P. R., Bessell, M. S., and Fox, M. W. 1981, *Ap. J.*, **272**, 99.
 Young, E. T., Neugebauer, G., Kopan, E. L., Benson, R. D., Conrow, T. P., Rice, W. L., and Gregorich, D. T. 1985, *A Users Guide to the IRAS Pointed Observation Products* (AO Guide) (IPAC report).
 Zhou, K., Hao, Y., Chen, P., Zhang, Y., and Gao, M. 1986, *Ap. Space Sci.*, **107**, 373.
 Zuckerman, B., Palmer, P., Gilra, D. P., Turner, B. E., and Morris, M. 1978, *Ap. J. (Letters)*, **220**, L53.

JEREMY MOULD, NEILL REID, and CHRIS TINNEY: Robinson Laboratory 105-24, California Institute of Technology, Pasadena, CA 91125